

## The tungsten-gold veins of Bonnac (French Massif central): new constraints for a Variscan granite-related genesis

Florent Cheval-Garabédian<sup>1,a,\*</sup>, Michel Faure<sup>1</sup>, Éric Marcoux<sup>1</sup> and Marc Poujol<sup>2</sup>

<sup>1</sup> Institut des Sciences de la Terre d'Orléans (ISTO), UMR 7327-CNRS/Université d'Orléans/BRGM, 1A, rue de la Férollerie, 45071 Orléans cedex 2, France

<sup>2</sup> Université de Rennes, CNRS, Géosciences Rennes – UMR 6118, 35000 Rennes, France

Received: 29 April 2020 / Accepted: 2 December 2020

**Abstract** – In the Brioude-Massiac district (French Massif Central: FMC), a network of W-As-Bi-Au quartz veins constitutes the Bonnac deposit, where tungsten is the major economic element, together with high-grade gold (up to 15 g/t Au). The evolution of this mineralization has been divided into 3 stages: (i) an early deep-seated wolframite-löllingite stage formed between 12 to 9 km, at up to 400 °C; (ii) a ductile/brittle deformation stage associated with scheelite and arsenopyrite deposition, with an estimated temperature of 480–300 °C; (iii) a late stage controlled by fluid-overpressure potentially triggered by fault-valve mechanism, at a depth of 7 to 5 km, and a temperature estimated between 266 to 240 °C, is marked by microfracturing infilled by native bismuth, bismuthinite, hedleyite, electrum, pyrite and base-metals. Structural analysis and apatite LA-ICP-MS U/Pb dating demonstrate a spatial and temporal link between the emplacement of the peraluminous leucogranitic dykes and the Bonnac mineralization. In more details, the mineralization was deposited between 321–316 Ma, during, or just after, the emplacement of the peraluminous dykes estimated around 329–315 Ma, suggesting a magmatic-hydrothermal transition for the ore-forming process. In the proposed model, the cooling of a hidden two-mica granitic pluton could have generated a magmatic fluid, and acted as the heat source responsible for fluid flow towards inherited permeability zones. The magmatic fluid could have then re-equilibrated at high temperature by fluid-rocks interaction. The sharp changes in pressure, associated with the decrease of the temperature, and sulfide-fugacity generated by a late input of meteoric fluid were responsible for the deposition of the late gold-stage. At the regional scale, the tungsten-gold event is ascribed to an early hydrothermal stage, dissociated from the formation of the antimony event in the district. The leucogranitic dykes and Bonnac quartz veins are controlled by a NW-SE stretching direction, interpreted as an expression of the Serpukhovian-Bashkirian syn-orogenic extension (D4 event of the FMC). These new data provide evidence for an early tungsten and gold metallogenic event in the FMC, prior the “Or300” event. The genetic classification of the Bonnac mineralization is equivocal. The W-As-Bi-Au-quartz veins exhibit the features of both an “orogenic gold” deposit at a relatively deep emplacement level (mesozonal), and an Intrusion-Related-Gold-Deposit (IRGD) type with a spatial-temporal link with the peraluminous intrusion emplacement. We propose that the Bonnac deposits represent an intermediate type between a typical orogenic-gold deposit and an IRGD. We argue that the presence of economic high-grade gold content in tungsten vein-type, and more generally the IRGD deposits, have been underestimated in the Variscan French Massif Central.

**Keywords:** Tungsten-Gold ore deposit / French Massif Central / IRGD / Variscan metallogeny / Brioude-Massiac district / Apatite U-Pb dating

**Résumé** – Les filons à tungstène-or de Bonnac (Massif central français) : nouvelles contraintes pour une genèse reliée aux granites varisques. Dans le district de Brioude-Massiac (Massif Central français; FMC), les gîtes de Bonnac correspondent à un réseau de veines de quartz à W-As-Bi-Au. Le tungstène y est le principal métal économique, et est associé à de fortes teneurs en or (entre 1 et 15 g/t Au). L'évolution de cette minéralisation peut être divisée en 3 étapes : (i) un stade précoce à wolframite et löllingite, formé en

\*Corresponding author: [florent-cg@hotmail.fr](mailto:florent-cg@hotmail.fr)

<sup>a</sup> Present address: Société Minière Georges Montagnat, 30, route de la Baie des Dames, 98800 Nouméa, Nouvelle-Calédonie.

profondeur, entre 12 et 9 km, et à des températures supérieures à 400 °C ; (ii) un stade de déformation ductile/cassant qui contrôle le dépôt de scheelite et d'arsénopyrite, estimé entre 480–300 °C ; (iii) un stade tardif, contrôlé par des surpressions de fluide marquées par une micro-fracturation colmatée par une paragenèse à bismuth natif, bismuthinite, hedleyite, électrum, pyrite associée à des métaux de base. Les surpressions de fluide seraient possiblement provoquées par un mécanisme de valve-sismique, à des températures comprises entre 266 et 240 °C, à une profondeur estimée entre 7 et < 5 km. L'analyse structurale, et les datations U/Pb sur apatite par la méthode LA-ICP-MS démontrent un lien spatial et temporel entre les dykes leucogranitiques peralumineux et les gîtes de la région de Bonnac. La formation de la minéralisation entre 321–316 Ma est contemporaine à légèrement plus jeune que celle des dykes peralumineux mis en place autour de 329–315 Ma, ce qui suggère une genèse lors d'une transition magmatique-hydrothermal. Dans ce modèle, le refroidissement d'un pluton granitique à deux micas sous-jacent, pourrait générer des fluides magmatiques et servir de source de chaleur activant une circulation du fluide vers des zones à haute perméabilité comme des fractures préexistantes. Le fluide magmatique aurait ensuite été rééquilibré à haute température par des processus d'interaction fluide-roches. Les changements brusques de pression, la baisse des températures, et de fugacité du soufre générés par un apport tardif de fluides météoriques semblent responsables du dépôt du stade aurifère tardif. À l'échelle régionale, l'événement or-tungstène est attribué à un stade hydrothermal précoce, et dissocié de la formation de l'événement à antimoine du district. La mise en place des dykes leucogranitiques et des veines de quartz de Bonnac est contrôlée par une direction d'étirement NW-SE, interprétée comme une expression de l'extension syn-orogénique d'âge Serpukhovien-Bashkirien (événement D4 du Massif Central français). Ces nouvelles données fournissent des preuves d'une première période métallogénique à tungstène et or dans le FMC avant l'événement « Or 300 ». La classification génétique des minéralisations de Bonnac est équivoque. Les veines de quartz à W-As-Bi-Au présentent à la fois les caractéristiques du modèle de l'« or orogénique », avec un niveau relativement profond de mise en place (mésoszonal), et celles du modèle Intrusion-Related-Gold-Deposit (IRGD) avec un lien spatio-temporel entre la minéralisation et une intrusion peralumineuse. Nous proposons que Bonnac soit un type intermédiaire entre un modèle typique de l'or orogénique, et un IRGD. Nous soutenons que la présence de teneurs économiques en or dans les gisements de tungstène de type filonien, et plus généralement ceux de type IRGD, ont été sous-estimés dans la partie varisque du Massif Central Français.

**Mots clés** : minéralisation à tungstène-or / Massif Central français / IRGD / métallogénie Varisque / district de Brioude-Massiac / âge U-Pb sur apatite

## 1 Introduction

The French Massif Central (FMC) represents a prominent metallogenic province for gold (Bouchot *et al.*, 2005) but only a few tungsten deposits have been found, although resources of at least 45,000 t of WO<sub>3</sub> have been estimated (Audion and Labbé, 2012), this is probably the consequence of an under-exploration for this metal in the FMC. The ubiquity of the quartz-wolframite hydrothermal veins makes it the main source of tungsten in the FMC. Some deposits with still a strong economic potential were formerly mined, such as Leucamp, Engualès and Echassières (Marignac and Cuney, 1999; Fig. 1).

Among the wolframite-bearing veins of the FMC, some display a polymetallic content with bismuth and gold in sub-economic grade (W-As-Bi-Au). They are ascribed either to the perigranitic wolframite vein-type (Marignac and Cuney, 1999) or to orogenic gold deposit (Bouchot *et al.*, 2005). In the FMC, occurrences of W-As-Bi-Au are known in gold mining districts such as the Limousin (Marcoux and Bonnemaison, 1988), Pontgibaud (Marcoux and Picot, 1985), Brioude-Massiac (Périchaud, 1970; Bril, 1982; Marcoux and Bril, 1986; Sandras, 1988; Bril and Beaufort, 1989; Bril *et al.*, 1991), Montredon (Béziat *et al.*, 1980), St-Mélany (Charonnat, 2000; Chauvet *et al.*, 2012), and Leucamp districts (Derré, 1983; Bogdanoff *et al.*, 1987; Demange *et al.*, 1988; Bouchot *et al.*, 2005; Leroux and Bouchot, 2009). The spatial association of

the wolframite-quartz veins with Carboniferous peraluminous two-mica granites argues for an important role of this crustal magmatism in the genesis of the tungsten mineralization (Marignac and Cuney, 1999; Cuney *et al.*, 2002; Bouchot *et al.*, 2005; Harlaux *et al.*, 2018). However, the formation of these peri-granitic deposits is still debated. In particular, the temporal and genetic links between the episodes of magmatism, deformation, and hydrothermal mineralization are not fully clarified.

U-Pb TIMS dating on wolframite from the Limousin, Echassières, Montredon, and St-Mélany districts (Fig. 1) has been recently performed (Harlaux *et al.*, 2018). The obtained U-Pb ages define the existence of three tungsten mineralizing events closely related to magmatic activity:

- Visean to Serpukhovian mineralization (333–327 Ma) coeval with the emplacement ages of large peraluminous two-mica plutons (ca. 335–325 Ma) during the syn-orogenic extension;
- Serpukhovian to Bashkirian mineralization (317–315 Ma) synchronous with the emplacement of syn-tectonic granites (ca. 315–310 Ma) during the late-orogenic extension;
- Gzhelian to Asselian mineralization (around 300–298 Ma), formed during the post-orogenic extension, coeval with the metallogenic peak of the Or300 event during which the main orogenic gold deposits were emplaced in the FMC (Bouchot *et al.*, 2005).

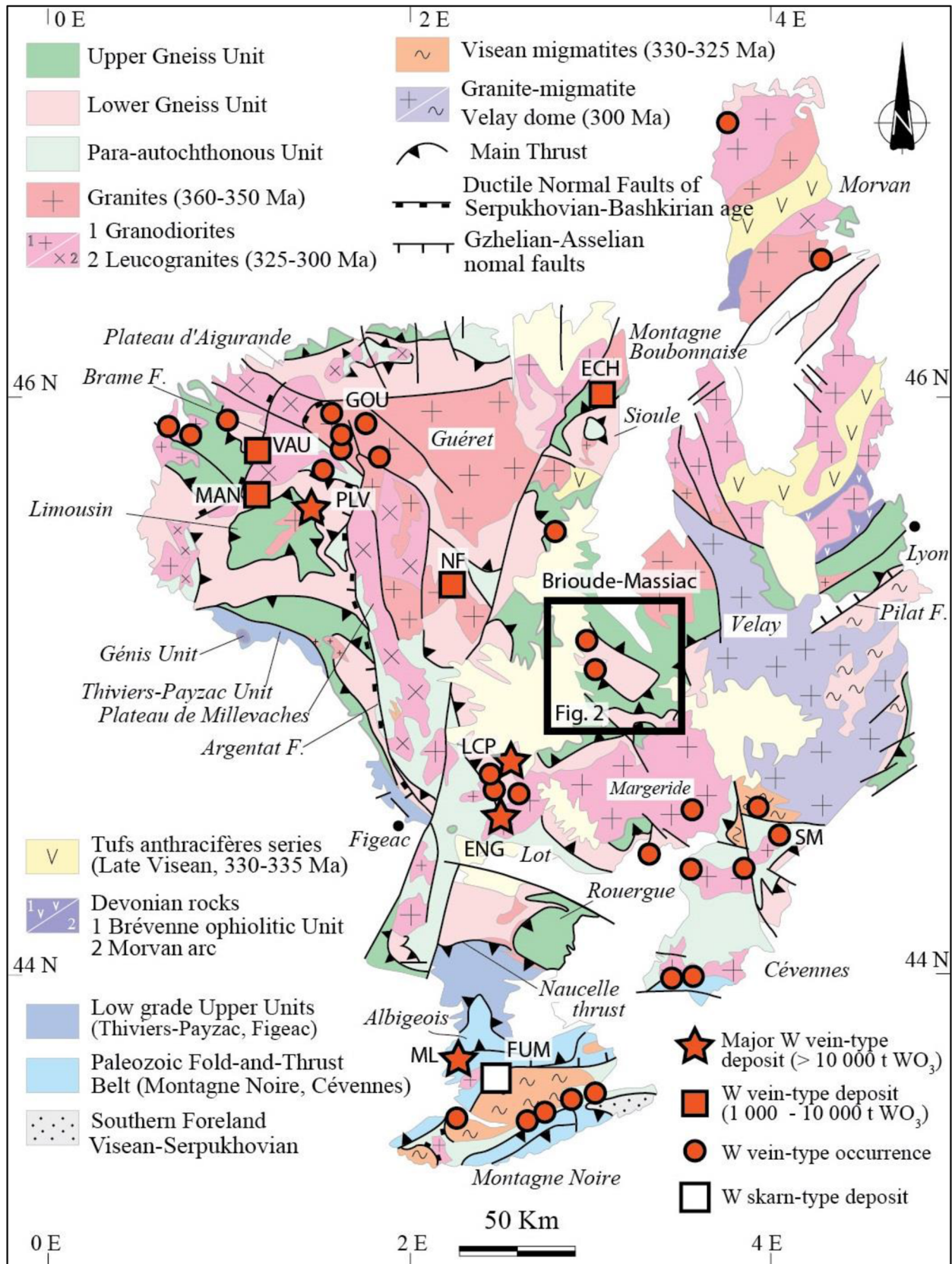


**Fig. 1.** Geological map of the French Massif Central (modified from Faure *et al.*, 2009), with the location of, the tungsten deposits and occurrences (from Audion and Labbé, 2012), and the study area. Tungsten district name abbreviations: ECH: Echassières; ENG: Engualès; FUM: Fumade; GOU: St-Goussaud; LCP: Leucamp; MAN: Mandelèsse; ML: Montredon-Labessonniè; NF: Neuf-Jours; PLV: Puy-les-Vignes; SM: St-Mélany; VAU: Vaulry.

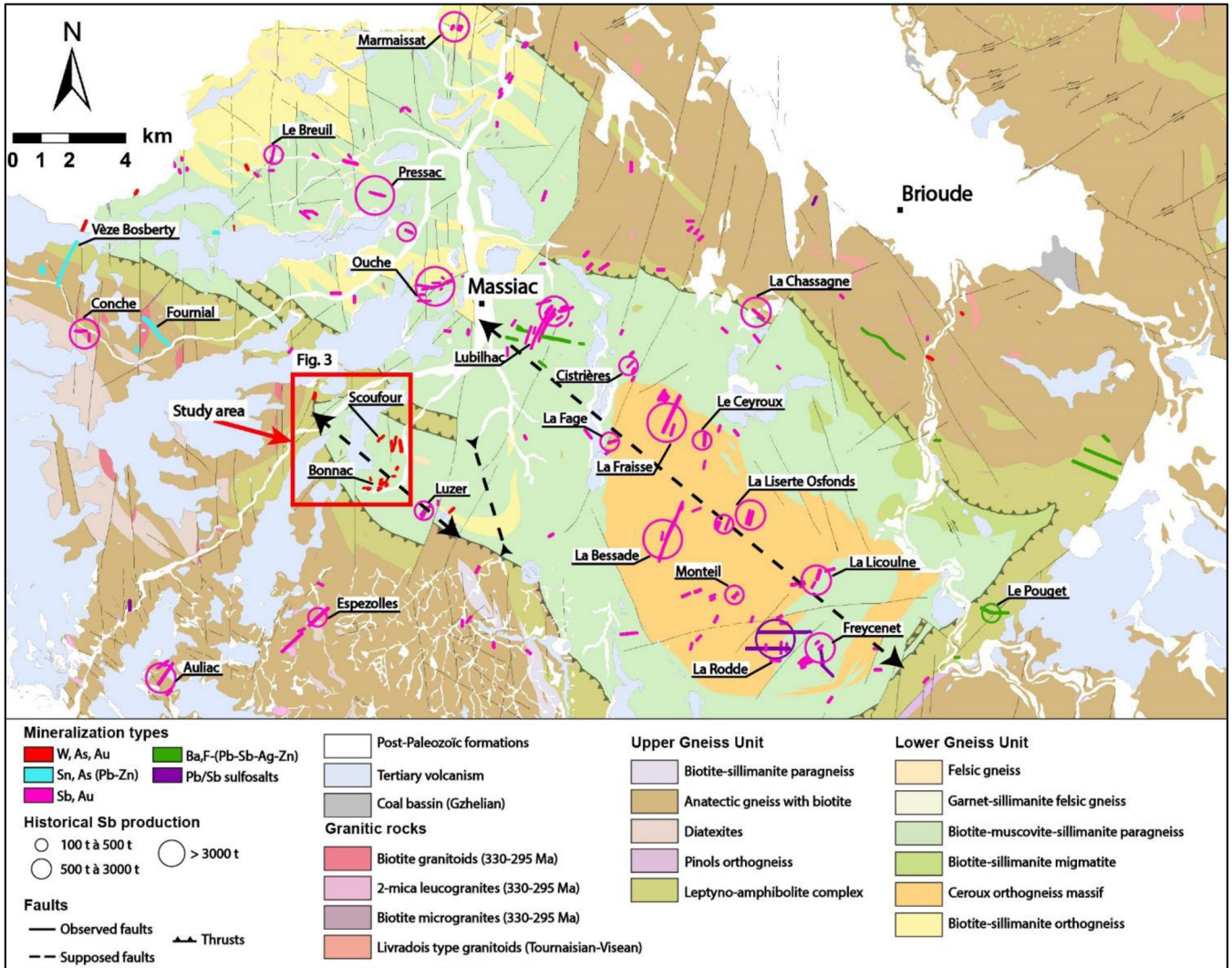


**Fig. 2.** Location of the study area within the geological and metallogenic framework of the Brioude-Massiac district. The simplified geology modified from Lasnier *et al.* (1982) and Thonat *et al.* (2014). Location and extension of mineralized veins are from Périchaud (1970).

In the central part of the FMC, *i.e.* in the Pontgibaud, Brioude-Massiac, and Leucamp districts, the timing for the emplacement of the wolframite-bearing veins remains poorly constrained. Furthermore, the genetic relationships between the ore deposits and the granitic emplacement is not yet demonstrated. The Bonnac area, in the central part of the Brioude-Massiac district is a good target to address these questions (Fig. 1). Indeed, in this area, a dozen of W-As-Bi-Au bearing quartz veins from the South of the Bonnac village to the Scoufour hamlet (Fig. 3) further north (Périchaud, 1970; Sandras, 1988) are spatially associated with a leucogranitic dyke swarm dated at  $322 \pm 7$  Ma (K/Ar on muscovite, Bril *et al.*, 1991), while the W-As-Bi-Au mineralization yields late Permian age of about 250 Ma (K/Ar on muscovite from Bonnac; Bril *et al.*, 1991). Variable gold grades ranging from 1 to 15 g/t have been reported in ore samples from the region (Périchaud, 1970; Sandras, 1988), but the relationship between gold and tungsten ore is not clearly documented.

The aim of this study is to better understand the W-As-Bi-Au quartz vein deposits in the FMC, and more particularly in

the Bonnac area. It focuses on the structural control and the timing of these ore deposits, and their relationships with the Carboniferous tectonics and magmatism, and will be integrated within the hydrothermal framework of the Variscan FMC. Detailed field structural studies, and *in situ* apatite LA-ICP-MS U/Pb dating were carried out. Mineralogical and geochemical studies were also performed to decipher the tungsten-gold relationships and propose an updated metallogenic model.

## 2 Geological and metallogenic background

### 2.1 The Haut-Allier area in the FMC Variscan framework

Located in the central part of the FMC, the 1000 km<sup>2</sup> Brioude-Massiac polymetallic district is covered by Cenozoic basaltic flows, and bounded to the northeast by the Oligocene Limagne graben. The district that belongs to the Variscan orogen, is a N120–130°E trending antiform that refolds the

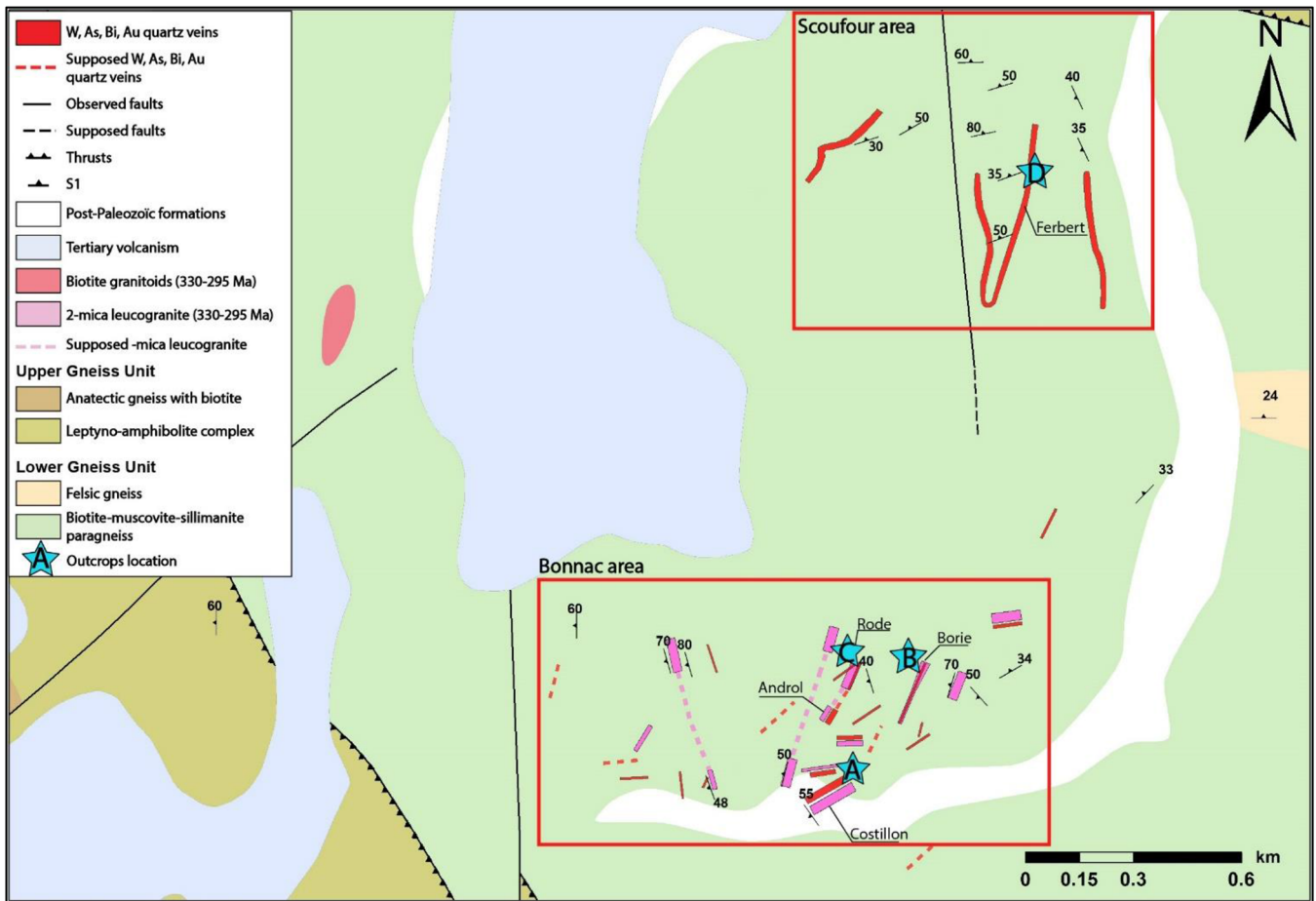


**Fig. 3.** Geological and structural map of the Bonnacc area with the location of most interesting outcrops.

stack of metamorphic nappes recognized in the entire Massif Central (*e.g.* Burg and Matte, 1978; Ledru *et al.*, 1989; Faure *et al.*, 2005, 2009; Figs. 1 and 2). The core of the area is occupied by the Lower Gneiss Unit (LGU) represented by biotite-sillimanite paragneiss, intruded by the Céroux orthogneiss derived from a Cambro-Ordovician alkaline granite (Burg and Matte, 1978; Lasnier *et al.*, 1982; Mathonnat, 1983; Thonat *et al.*, 2014). The LGU is tectonically overlain by the Upper Gneiss Unit (UGU), which is formed by migmatitic paragneiss with rare orthogneiss, and a felsic-mafic association called the “leptynite-amphibolite complex”. The mafic rocks experienced an eclogite-facies or granulite-facies metamorphism during the eo-Variscan evolution (Marchand, 1974; Lasnier, 1977; Bernard-Griffiths *et al.*, 1980).

The nappe stacking in the Haut-Allier area was probably acquired during the early Carboniferous, around 350–340 Ma (monazite U/Pb dating on syntectonic granulite; Pin and Peucat, 1986). Then two extensional events, coeval with granitic intrusions accommodated the crustal thinning widely observed in the FMC (*e.g.* Malavieille *et al.*, 1990; Faure and Pons, 1991; Faure, 1995):

- the syn-orogenic extension at ca 330–310 Ma, called D4 event (Faure *et al.*, 2009), is characterized by a NW-SE maximum stretching recorded by the syn-tectonic biotite monzogranite and the two-mica granite plutons and

their country rocks. In the Brioude-Massiac area, andalusite-leucogranitic dykes and their related two-mica granites (Sandras, 1988; Bril *et al.*, 1991) belong to this D4 event;

- the late-orogenic extension (D5 event, between 310 to 299 Ma; Faure *et al.*, 2009), with a NNE-SSW maximum stretching direction, was contemporaneous with the emplacement of highly differentiated peraluminous intrusions and pegmatites, and rare-metal granites (Cuney *et al.*, 2002). The opening of the Late Carboniferous coal basins belongs to the D5 event (Faure, 1995).

## 2.2 The Bonnacc W-As-Bi-Au deposits

The study area is located in the central part of the Brioude-Massiac polymetallic district which contains more than 200 veins-type deposits and occurrences with variable ore content: W, Sn or W-As-Bi-Au (Bonnacc, Vèze-Bosberty veins), Sb (Au), Pb-Zn or F and Ba (Fig. 2). Antimony veins have been the main economic substance mined between 1850 and 1978 with an historical production of 43 000 t Sb metal (Périchaud, 1970; De Gramont *et al.*, 1990). The Bonnacc area was only mined for gold between 1880 and 1911 with a production of only 2 kg of gold, and never for tungsten (Périchaud, 1970; De Gramont *et al.*, 1990).

The Bonnac W-As-Bi-Au quartz-veins are spatially associated with Sb (Au) quartz veins (Fig. 2) and are located in the southwestern limb of a regional N120–130°E antiform. All veins seem to crosscut the foliation of the LGU paragneiss (Figs. 2 and 3). Some quartz veins develop immediately at the contact with andalusite leucogranitic dykes (Périchaud, 1970; Sandras, 1988). The ore mineralogy, is mainly represented by arsenopyrite-löllingite with wolframite, minor scheelite, associated with bismuthinite, native bismuth, tetradymite and visible gold in a quartz gangue with muscovite clusters (Périchaud, 1970; Bril, 1982; Bril and Beaufort, 1989).

Detailed studies on fluid inclusions (Bril, 1982), hydrothermal alteration (Bril and Beaufort, 1989), and lead isotopic signature (Marcoux and Bril, 1986) allow to constrain the P-T conditions of vein deposition. The Bonnac veins display two successive hydrothermal stages with an early high temperature (homogenization temperatures between 350–400 °C) CO<sub>2</sub>-CH<sub>4</sub>-rich ± N<sub>2</sub> aqueous fluid with low-salinity (about 5 equiv wt % NaCl), interpreted as of metamorphic origin, and a late low temperature (homogenization temperatures between 200–300 °C) aqueous fluid, with low-salinity, of meteoric origin, similar to the ore forming fluid from the Sb (Au) deposits. According to the same authors, the formation of the W-As-Bi-Au and Sb (Au) veins could be contemporaneous, the result of a single hydrothermal system coeval with the emplacement of an underlying, albeit hidden, Permian pluton. The ore veins were considered to show a zonal distribution, with W-As-Bi-Au occurring in a limited area, near the intrusion, the Sb (Au) veins being more distal.

### 2.3 The intrusive rocks

Leucogranitic dykes, striking N30°E, N60°E and sometimes N100°E, with a variable thickness (between 50 cm to 20 m), and small extension (less than 3 km), are cropping out in a few clusters in the district, the Bonnac area being one of the most important (Figs. 2 and 3). These dykes display a homogeneous mineralogical and chemical composition in the overall district (Sandras, 1988). Quartz is the most abundant mineral, associated with plagioclase, and sub-euhedral K-feldspar (<5 mm) with biotite aggregates and muscovite. Andalusite is observed as small sized grains (0.6 to 0.8 mm), associated with the K-feldspar and quartz. A temperature emplacement of ca 600–650 °C, and a pressure of 0.4 GPa, was estimated from the andalusite-quartz assemblage (Sandras, 1988). An emplacement age of 322 ± 7 Ma was documented by K/Ar radiometric dating on muscovite (Bril *et al.*, 1991).

The dykes chemical compositions correspond to a peraluminous two-mica granite with 74 to 76% SiO<sub>2</sub>, and a Al<sub>2</sub>O<sub>3</sub>/CaO + Na<sub>2</sub>O + K<sub>2</sub>O ratio up to 1.6 (see EDM. 1 for analytical details). This bulk chemistry is similar to those found in the Chatelet gold district, and other Visean to Serpukhovian leucogranites from the Limousin district (*e.g.* St-Sylvestre massif; Scaillet *et al.*, 1996). A local partial melting of the LGU paragneiss could be responsible for the genesis of those intrusive rocks (Sandras, 1988). A spatial and potentially genetic link with the W-As-Bi-Au deposits of the Brioude-Massiac district is assumed. At Bonnac, the dykes are interpreted as the shallow expression of an underlying pluton (Sandras, 1988; Bril and Beaufort, 1989).

## 3 Materials and methods

The accessory mineral phases were identified using a Merlin compact Zeiss Scanning Electron Microscopy (SEM), co-operated by BRGM-CNRS-Orléans University, and equipped with Energy Dispersive System (EDS) for qualitative analyses. In addition, SEM-cathodoluminescence images have been made using MEB-CL MIRA-3 Tescan (BRGM-CNRS-Orléans University). Chemical analyses of arsenopyrite were obtained with the Cameca SX-Five Electron Probe Micro-Analyzer (EPMA) at the Institut des Sciences de la Terre d'Orléans (ISTO). Analyses were performed using an accelerating voltage of 20 kv, a beam current at 40 nA, a beam diameter of 3 µm, and a counting time of 30 s for Fe, Ni, Co, Sb, Pb, Cu, As, Zn, Ag, Bi, and 60 s for gold. Details on the method, parameters and analytical data are given in ESM2.

U/Pb dating on hydrothermal apatite from the mineralization was conducted *in situ* by laser ablation inductively coupled plasma mass spectrometry (LA-ICP-MS) at the GeOHeLiS analytical platform (Géosciences Rennes/OSUR, Univ. Rennes) using an ESI NWR193UC Excimer laser coupled to an Agilent 7700 × quadrupole ICP-MS equipped with a dual pumping system to enhance sensitivity (Paquette and Piro, 2014). The analytical procedure followed the method described in Pochon *et al.* (2016). Details, standards analyses and analytical data are provided in ESM3. All errors are listed at 2σ level. Concordia diagrams and calculated ages have been produced using IsoplotR (Vermeesch, 2018).

## 4 Field characterization of the W-As-Bi-Au quartz veins

### 4.1 Field and structural features from the Bonnac area

The strike of the mineralized quartz veins displays four different orientations similar to those of the leucogranitic dykes. The N30°E trend is represented by the Riolet, Androl, Rode, Borie veins), the N60°E by the Costillon one, while few veins strike N90°E and N160–170°E (Fig. 3). The vein dip varies between 30° to 45° to the SE whatever their strike. Mineralized quartz veins are located in the hangingwall or footwall of the leucogranitic dykes (Figs. 4 and 5). They display similar features all around the area, with a lenticular shape, and a narrow width of 1 to 20 cm. The host-rocks are weakly affected by the hydrothermal alteration. The geometric relationships show that the leucogranitic dykes crosscut the paragneiss foliation, and are cut by the mineralized veins (Figs. 4 and Figs. 4B and 5) with locally developed breccias (Fig. 4B).

Most of the vein wallrocks are fault planes with a down-dip striation, indicating a normal motion (Fig. 5). Some veins display also a striation with a NE 40–50° pitch, in which quartz steps indicate a normal component of displacement (Fig. 5C, D). The observed kinematics of the Costillon vein (Fig. 4A) also indicate a normal motion that complies with the drag folds asymmetry developed around the leucogranitic dykes (Fig. 5B). Late N60–65°E striking sub-vertical barren faults, with gouge, offset the quartz veins (Fig. 4A).

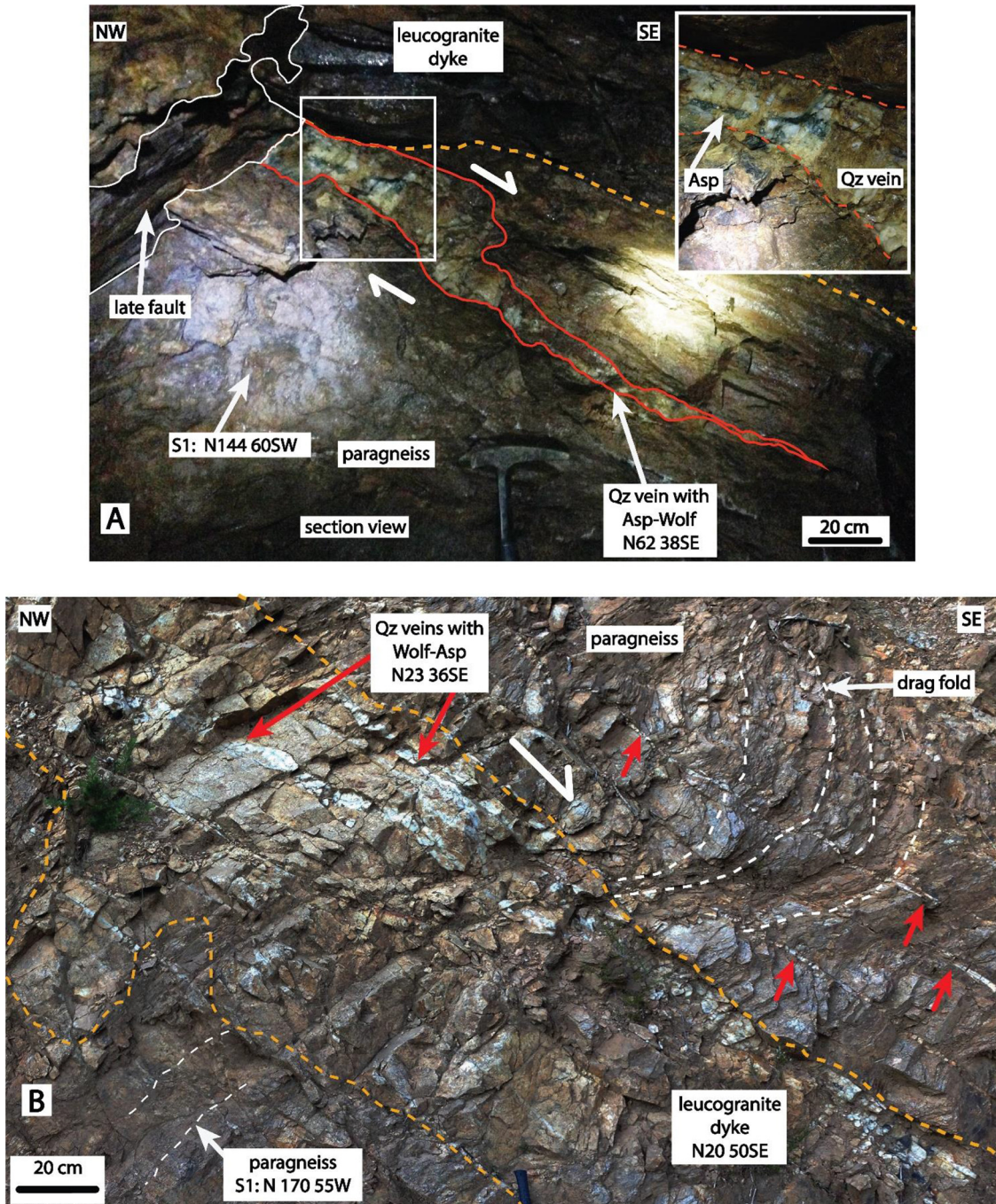


**Fig. 4.** (A) Representative arsenopyrite (Asp) and wolframite (Wolf) bearing quartz vein from the Costillon vein (outcrop A in Fig. 3) showing the structural features and the relationships with the paragneiss host-rock and the leucogranitic dykes. (B) Detail of drag folds developed in the country-rock paragneiss along the contact between the arsenopyrite (Asp) and wolframite (Wolf) bearing quartz veins and leucogranitic dyke. La Borie vein (outcrops B in Fig. 3).

#### 4.2 Field and structural features from the Scoufour area

The Scoufour mineralized quartz veins exhibit some differences with the Bonnac ones. Three N10–30°E striking low-angle veins with a dip between 10 and 20° to the SE are observed (Fig. 6). Their thickness is comprised between 30 and 50 cm, but may exceed 1 m. Here, leucogranitic dykes are absent, and the host-rock underwent a hydrothermal

alteration related to the mineralization. A greisen-type alteration is thus observed up to 1 or 2 m from the vein, resulting in the bleaching of the paragneiss by transformation of biotite into muscovite with associated silicification. Drag folds observed near the Ferbert vein show a normal motion (Fig. 6B). A late fracturing event, represented by N20–25°E steeply NW dipping barren faults with gouge, is also recognized (Fig. 6A).

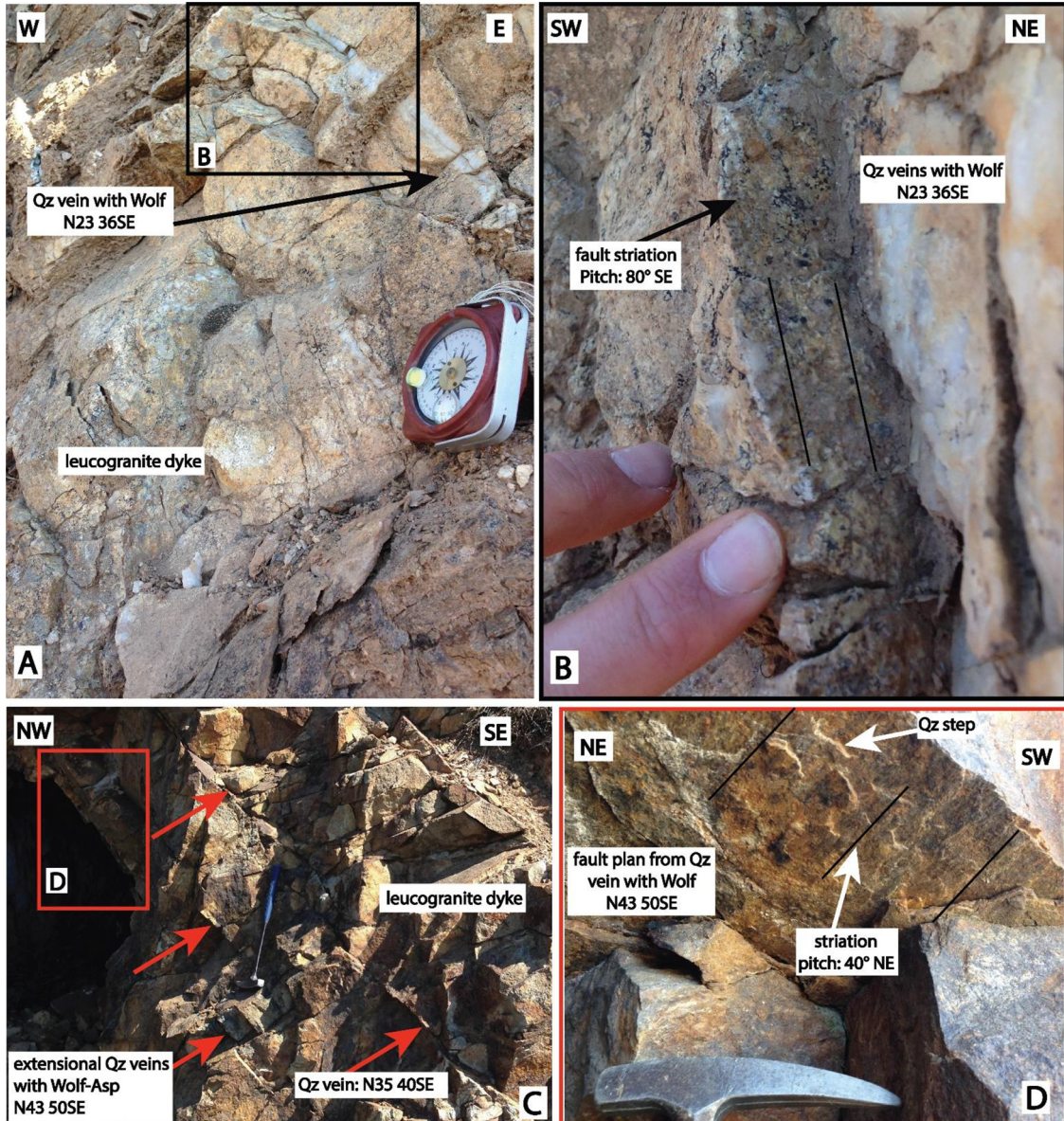


**Fig. 5.** (A) Detail picture of the [Figure 4B](#) W-As-Bi-Au bearing quartz vein crosscutting leucogranitic dykes (La Borie vein, outcrops B in [Fig. 3](#)). (B) Fault plane seen on [Figure 5A](#) with high angle pitch striation. (C) Cm-sized mineralized quartz veins network crosscutting the leucogranite dyke (the Rode vein, outcrops C on [Fig. 3](#)). (D) Focus on the fault plane in the mineralized vein of the [Figure 5C](#) showing a normal kinematics.

All the structural features observed in the Bonnac and Scoufour areas are summarized in [Figure 7](#). In both cases, the emplacement of the mineralized quartz veins occurred during a single deformation phase coeval with a hydrothermal event. The magmatic event responsible for dyke emplacement postdated the regional metamorphism but preceded the ore veins emplacement. Furthermore, normal faults rework the pre-existing faults that controlled the emplacement of the leucogranitic dykes. Lastly, both dykes and mineralized veins are cut by NE-SW subvertical faults with subhorizontal striation indicating a sinistral motion.

## 5 Mineralogy and geochemistry of the W-As-Bi-Au ore veins

### 5.1 The mineralized facies

All the mineralized veins of the study area have similar habitus, with a massive infill of coarse white-grey quartz gangue with parallel ribbons of a few centimeters, or aggregates of arsenopyrite and coarse wolframite ([Figs. 4A](#) and [8](#)). Secondary scheelite is common in cm-scale pseudomorphic aggregates of early wolframite that may

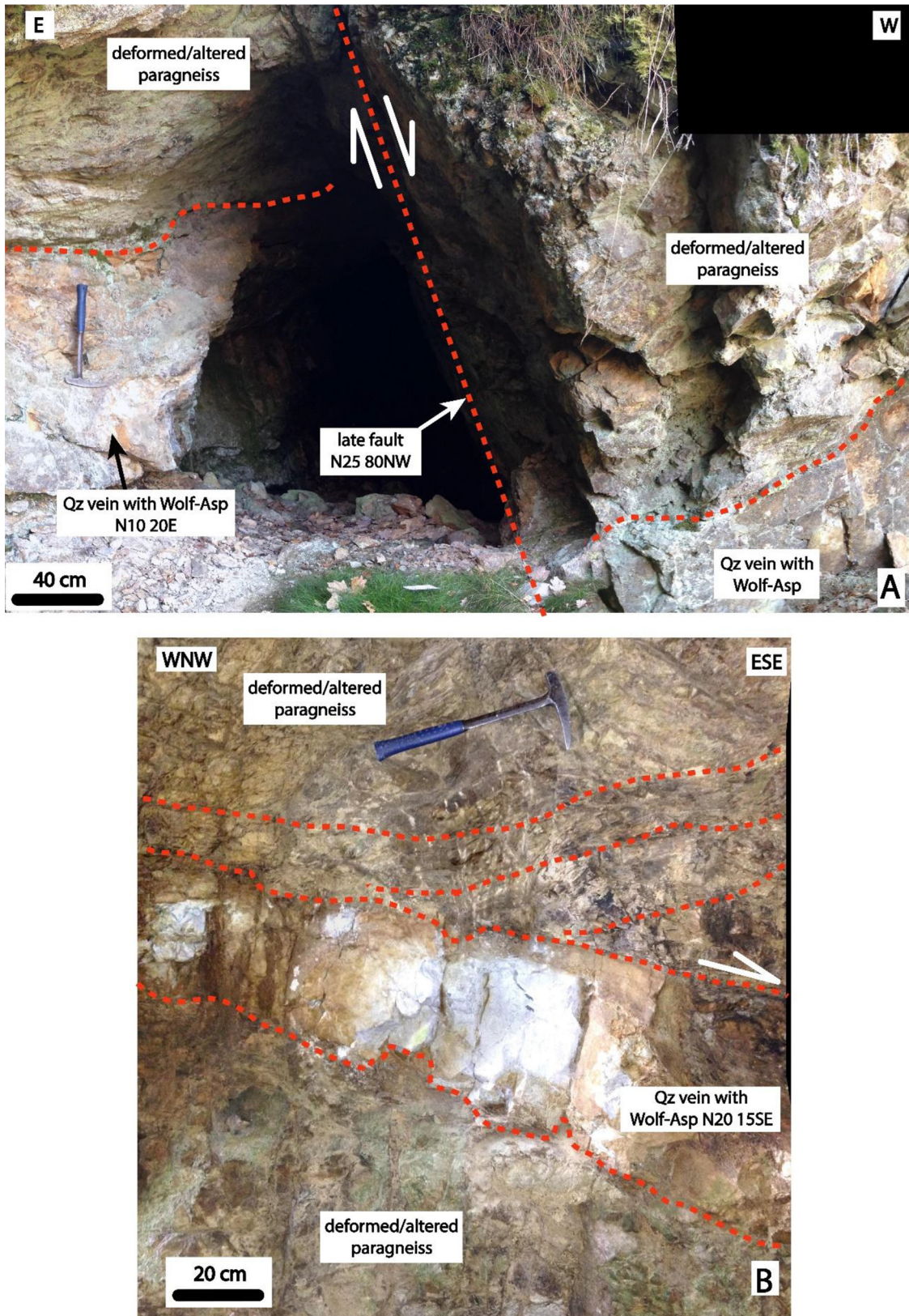


**Fig. 6.** Mine gallery opened in the Ferbert vein. (A) Low angle wolframite (Wolf) and arsenopyrite (Asp)-bearing quartz vein (outcrops D in Fig. 3). The vein is cut by late sub-vertical barren fault. (B) Detail of the quartz vein showing normal kinematics.

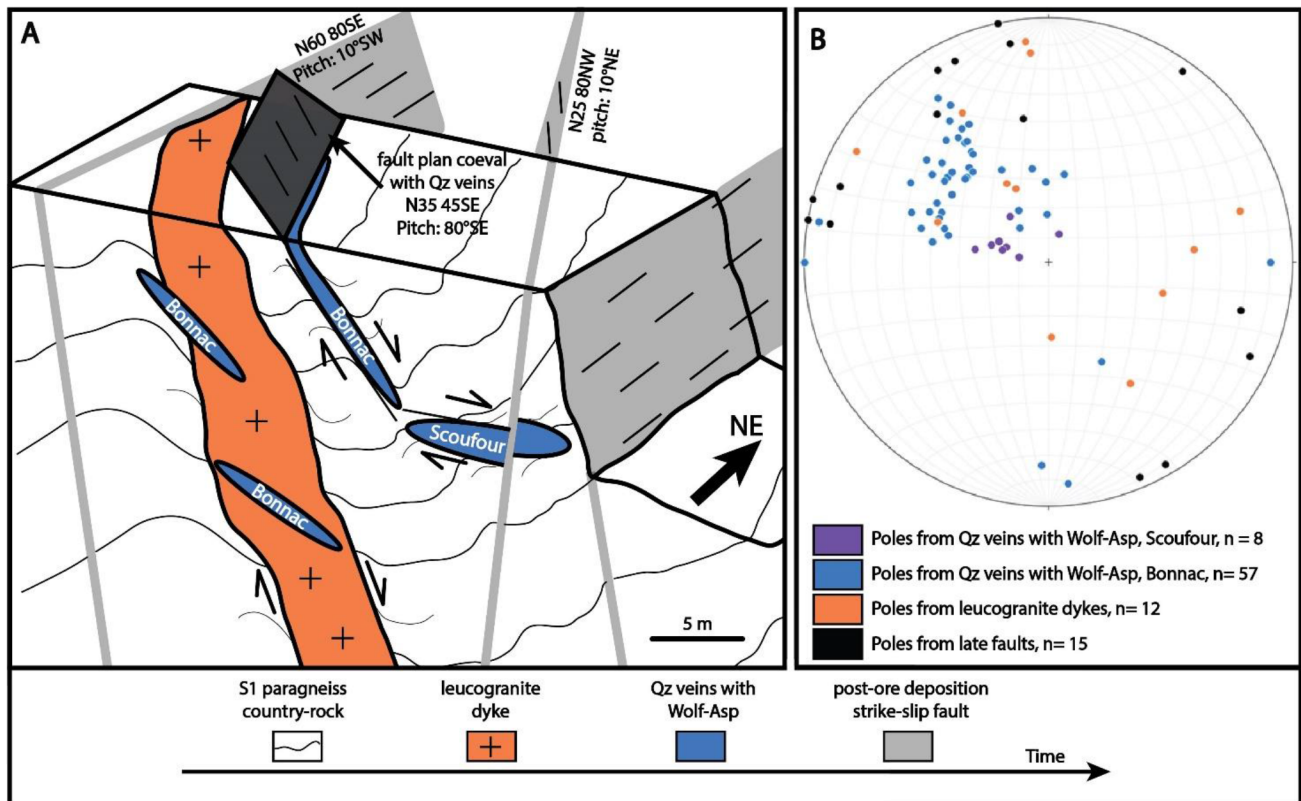


**Fig. 7.** (A) 3D block showing the main structural observations made on the mineralized quartz veins from Bonnacc area. They allow us to propose a relative chronology of the structures developed in the paragneissic host-rock, the leucogranitic dykes and the quartz veins. (B) Stereogram (lower hemisphere projection) of the poles of the fault planes coeval with the emplacement of the mineralized veins, leucogranitic dykes, and late faults measured in the field.

appear as rare relicts and rarely observed as isolated, coarse grains or infilling fractures (Fig. 8).

On the basis of gangue and ore mineral textural observations, 3 stages have been recognized, namely:

- stage 1 with tungsten and arsenic;
- stage 2 with arsenic, and tungsten;
- stage 3 with bismuth, gold, and base metals.

## 5.2 Stage 1: early tungsten and arsenic

The first opening of the veins corresponds to the deposition of a wolframite and löllingite assemblage in a macrocrystalline Qz1 quartz (crystal size  $>500\ \mu\text{m}$ ; Fig. 9A, B). Observed with cathodoluminescence, Qz1 displays a blocky habitus with regular growth bands without significant deformations (Fig. 9B), and numerous fluid inclusions. Coarse euhedral wolframite crystals (up to 1 cm) are associated with cm-size aggregates of löllingite (Fig. 9A). SEM analyses of wolframite exhibits a high iron grade (6–8 wt %) and a lower manganese one suggesting a ferberite. Large apatite crystals ( $>100\ \mu\text{m}$ ) have been observed within Qz1 in close association with wolframite (Fig. 9C). Their euhedral shape and straight grain boundaries suggest it is coeval with Qz1.

## 5.3 Stage 2: arsenic and late tungsten

The beginning of stage 2 is marked by an intense and heterogeneous episode of deformation (Fig. 9A–D), which has affected the previous stage 1 assemblage. Qz1 grains experienced a dynamic recrystallization (Stipp *et al.*, 2002) shown by undulose extinction, subgrain rotation and recrystallization with golfed or jagged shape of the Qz1 boundary, bulging and quartz neograin (Qz2) formation at the expense of the early Qz1 (Figs. 9B, D and 10A and B). Qz2 displays undulose extinction and grain size reduction and is located along 10 to more than  $500\ \mu\text{m}$  shear bands that surround the edges of Qz1, or crosscut it.

The crystallization of arsenopyrite (Fig. 9B) and scheelite are coeval with the deformation episode. Arsenopyrite forms small rhombic crystals (up to  $100\ \mu\text{m}$ ) and fills the fracture network of the stage 1 löllingite or wolframite and sometimes totally pseudomorphs after löllingite. Xenomorphic scheelite forms at this stage by partial or total pseudomorphosis of previous wolframite (Fig. 9A, C). The scheelites, show rare inclusions of niobium oxides rich in niobium as on the Ferbert vein (65 wt %  $\text{Nb}_2\text{O}_5$ ), iron (25 wt % FeO), manganese (4.5 wt % MnO), tungsten (2.4 wt %  $\text{WO}_3$ ), titanium (2.2 wt %  $\text{TiO}_2$ ) and scandium (0.9 wt %  $\text{Sc}_2\text{O}_3$ ). Those uncommon oxides have been observed in the Puy-les-Vignes tungsten deposit (Harlaux *et al.*, 2015).

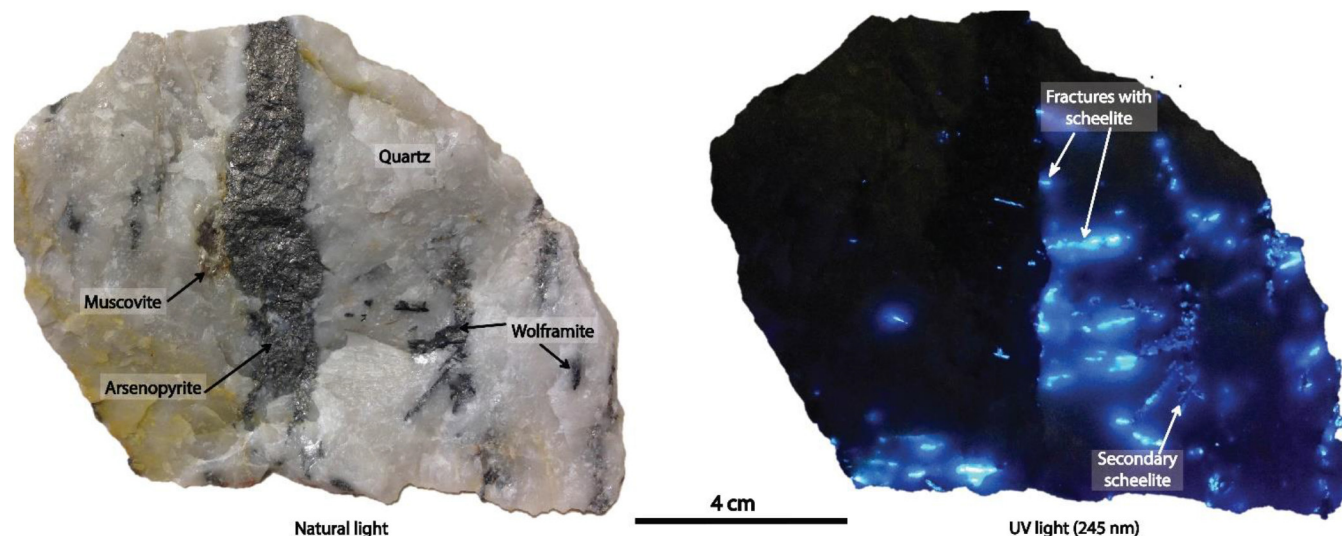


**Fig. 8.** Representative W-As-Bi-Au-bearing quartz hand sample from the Androl vein (see Fig. 3 for localization), with arsenopyrite, wolframite, scheelite, and muscovite. Sample is observed in natural light (left) and UV light (254 nm, right).

The 56 EPMA analyses of arsenopyrite (see Tab. 1 and ESM 2 for detail) have been compared with previous study of Brill (1983) from the Bonnac area and from other W-As-Au regional veins (Vèze and Bosberty, see Fig. 2 for localization). Arsenopyrite has a very similar composition in all deposits with As % average values of 33.4%, 32.8%, and 33.0% for Bonnac, Vèze, and Bosberty veins, respectively. Minor elements, *e.g.* Co, Ni, Sb, Au are under the detection limit of the method. According to Kretschmar and Scott (1976), and Sharp *et al.* (1985), the use of the arsenopyrite chemical compositions to assess ore formation temperatures may be considered with a good confidence level, because of the absence of minor element. Assuming the arsenopyrite-pyrrhotite equilibrium, the calculated formation temperature was around 480 °C. These values are in the same range than those deduced from the H<sub>2</sub>O-CO<sub>2</sub> L1-type fluid-inclusions (homogenization temperature between 300 and 420 °C; Brill, 1982).

#### 5.4 Stage 3: Bi-Te-Au and base metals

This stage is marked by the deposition of a new discrete quartz generation (Qz3) in the fractures of arsenopyrite or löllingite (Fig. 10C, D). The medium grain-size (around 100 μm) Qz3 displays a subeuhedral shape or elongate-fibrous habitus. Its hyaline aspect is due to the scarcity of fluid and solid inclusions. This Qz3 never experienced dynamic recrystallization (Fig. 10C, D) and is coeval with a bismuth-telluride-gold-base metals assemblage (Fig. 10C–E). Rhombic arsenopyrite crystals are commonly crosscut by large mm-size, subeuhedral pyrite, associated with bismuth-telluride and base-metals minerals (Fig. 11D, E). The EPMA chemical analysis of the pyrite from Bonnac veins does not show minor element.

Bismuthinite and native bismuth are the dominant minerals species of this stage 3. They occur as 2 to 80 μm inclusions aligned along the cleavage plane of löllingite (Fig. 11A), also within arsenopyrite, or wolframite (Figs. 10C, D and 11A–C), and as small-size aggregates (<500 μm) or in fractures

crosscutting löllingite or arsenopyrite (Fig. 10E, F). Native bismuth is frequently observed as ovoidal inclusions within bismuthinite (Figs. 10F and 11C). Xenomorphic hedleyite (Bi<sub>7</sub>Te<sub>3</sub>) is the main tellurium mineral, always closely associated with the bismuthinite and native bismuth. Tetrahedrite [(Cu,Fe)<sub>12</sub>Sb<sub>4</sub>S<sub>13</sub>] and a bismuth-antimony-sulfide, close to the chemical composition of the horobetsuite [(Bi,Sb)<sub>2</sub>S<sub>3</sub>], have been identified as inclusions in a hedleyite aggregate (Fig. 10F). In the Ferbert vein, a late deposition of Cu-Zn-Pb minerals overprints and brecciating all the previous minerals. Chalcopyrite is the main mineral, with small tetrahedrite inclusions (50 μm). Sphalerite and minor galena complete this assemblage. This late deposition stage is associated with a Qz4 quartz generation displaying undeformed pyramidal grains (Fig. 11E).

Visible gold has been commonly observed in thin-sections from all veins of the Bonnac area. Most of the gold intergrowths with the Bi-Te minerals (Figs. 10B and 11A–C), or more rarely appears within sulfides (mainly chalcopyrite, Fig. 11D, E), or sometimes pyrite or isolated between Qz2 grains. Gold patches range between 1 μm to 25 μm in size but can reach 50 μm within sulfides. All display a xenomorphous rounded shape (Fig. 11). Rare maldonite (Au<sub>2</sub>Bi) has been observed by SEM analysis as a few microns inclusions intergrowths with native bismuth.

Ten EPMA analyses of gold grains intergrowths with native bismuth and within chalcopyrite from the Ferbert vein are provided in Table 1 (see EDM 2 for detailed analyses). The small size of the gold grains explains why the analyses do not reach 100%. Silver is the only element present with gold (average of 16.7 wt % Ag). “Gold” of Bonnac area is thus an electrum with a gold fineness of 830 (Morisson *et al.*, 1991).

The three economic-stages described above are summarized in Figure 12, however, this evolution represents increments of a single progressive crystallization-deformation event.

It should be noted that, a poorly developed and uneconomic post-ore stage, macroscopically highlighted by a dark-gray quartz facies, has been only observed in the Ferbert

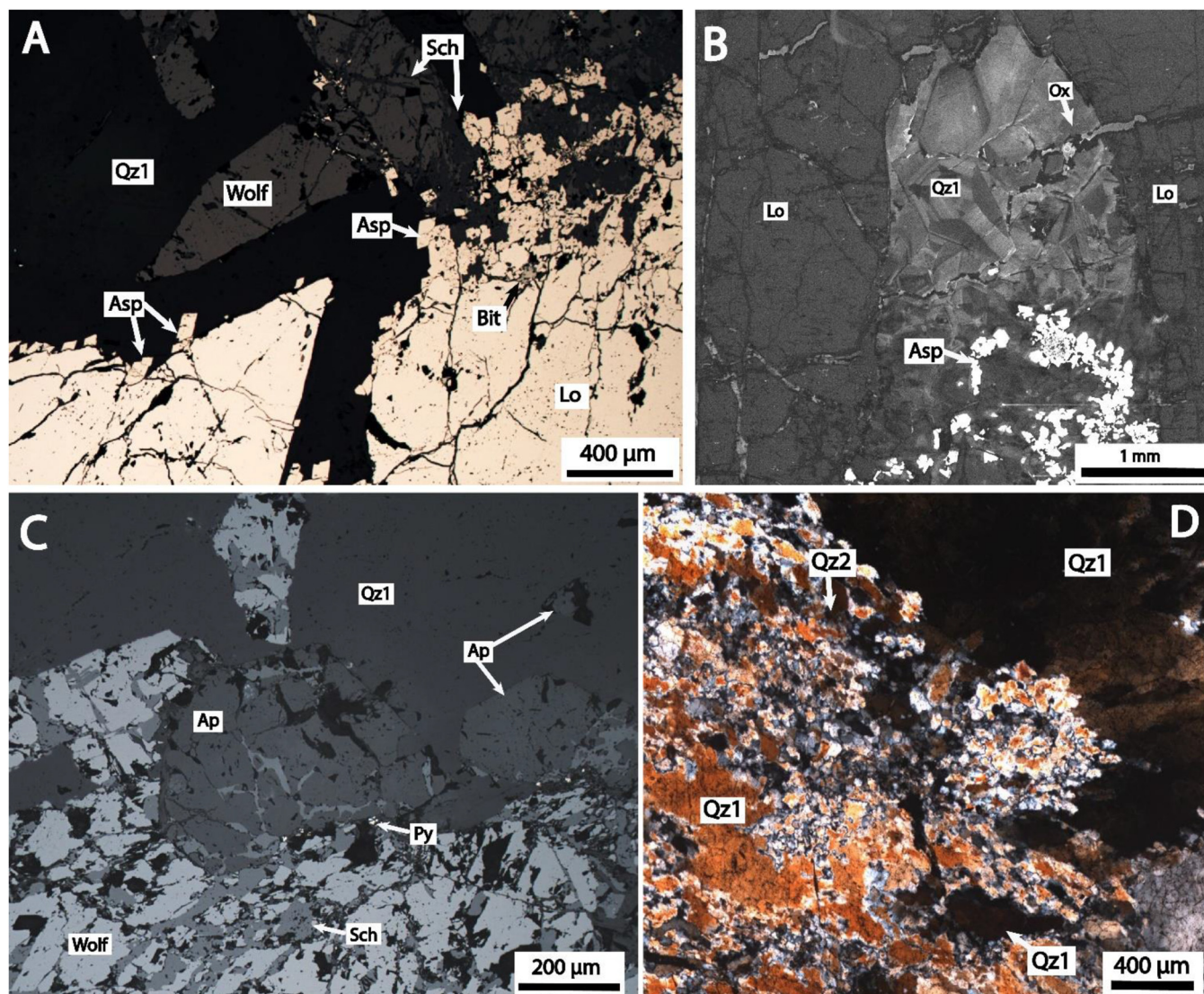


**Fig. 9.** Microphotographs showing the mineralogy of the stages 1 and 2 at Bonnac. (A) Coarse wolframite (Wolf) with lollingite (Lo) fractured and cemented by rhombic arsenopyrite (Asp). Secondary scheelite (Sch) pseudomorphs after wolframite. Arsenopyrite is fractured and cemented by bismuthinite (Bit) (Androl vein). (B) Cathodoluminescence view showing the relationships between lollingite (Lo), weakly deformed macrocrystalline quartz (Qz1), and arsenopyrite (Asp) rhombic crystals cutting Qz1 (Costillon vein). (C) Wolframite (Wolf) and coarse hydrothermal apatite (Ap) assemblage fractured and cemented by secondary scheelite (Sch) and minor pyrite (Py) (Ferberst vein). (D) Highly sheared macrocrystalline quartz (Qz1) crosscut by a second quartz generation (Qz2) (see text for further explanation). Relics of Qz1 clasts are present in the upper right part of the photograph (Ferberst vein).

vein. All the previous stages are brecciated and cemented by a chalcedonic quartz gangue with minor carbonates. The associated metallic-minerals are pyrite-marcasite aggregates with pyrrhotite relics, with a new generation of chalcocopyrite, and sphalerite. This does not greatly affect the previous assemblages.

## 6 LA-ICP-MS U/Pb geochronology on apatite

Hydrothermal apatite from the early tungsten-arsenic stage 1 (Figs. 9C and 12) of the Androl (Bonnac area) and Ferberst veins (Scoufour area) have been carefully characterized and 15 grains

have been selected for dating. Namely, 9 from the Ferberst vein (mineralized quartz vein sample BM46D) and 6 from Androl vein (mineralized quartz vein sample BM39A; ESM 3 for analytical details). The cathodoluminescence image shows growth zones without evidence complex zoning (Fig. 13A, B). Between 2 and 6 U/Pb analysis have been performed on each grain (Fig. 13C, D). Apatite grains from the Ferberst vein have variable  $^{207}\text{Pb}/^{206}\text{Pb}$  ratios, ranging between 0.1849 and 0.7010. The discordant points plot along a discordia line that yields a lower intercept date of  $315.6 \pm 2.8$  Ma (MSWD=3.7; Fig. 13C). The data plot along a discordia line yielding a lower intercept date of  $323.4 \pm 3.2$  Ma (MSWD=2.4, Fig. 13D). The intersect point of the discordia

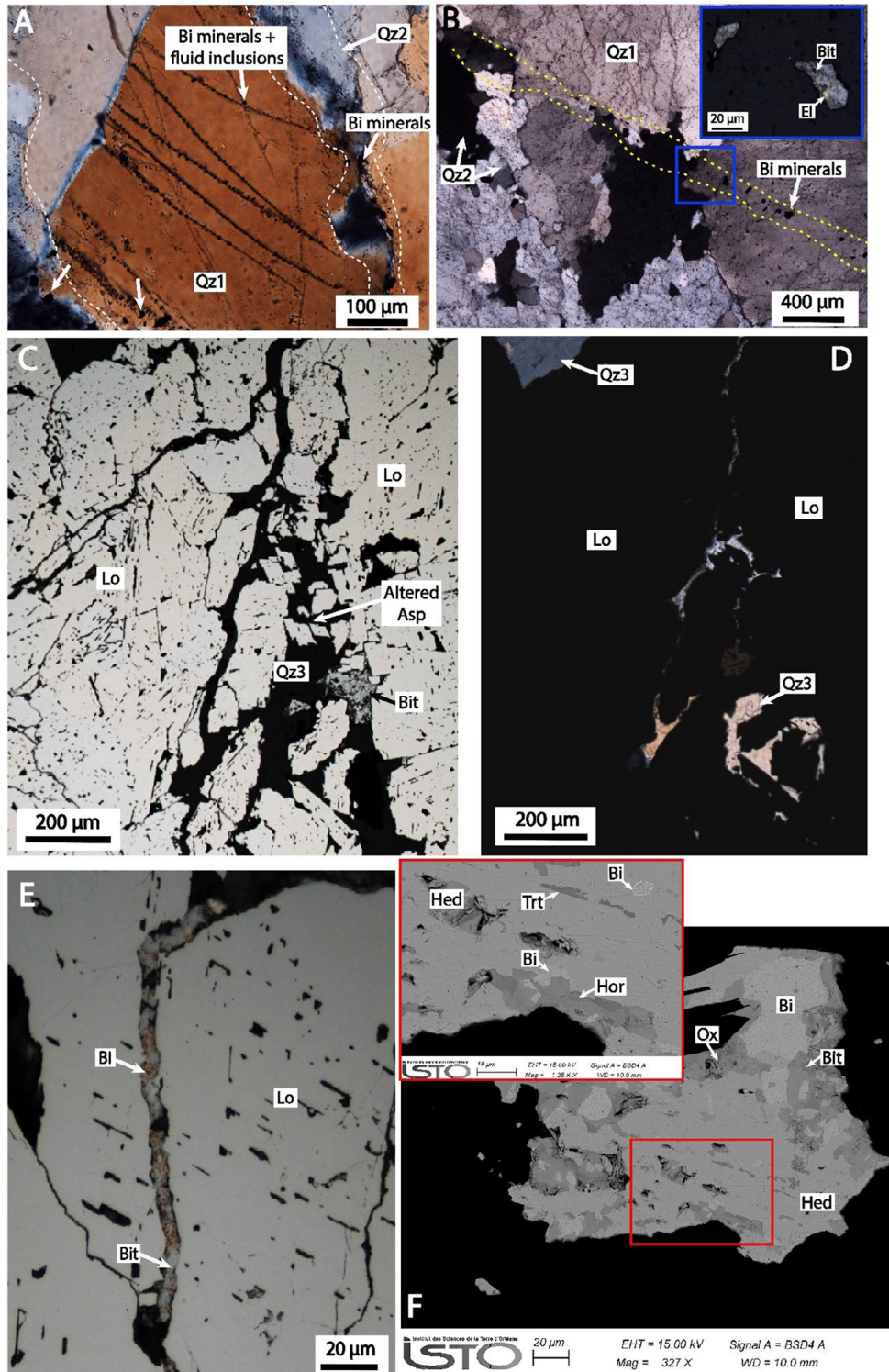


**Fig. 10.** Microphotographs showing the mineralogy of stage 3. (A) Macrocrystalline quartz (Qz1) and highly sheared quartz (Qz2) crosscut by microcracks with fluid inclusions and bismuth minerals (Bi minerals) (Ferberst vein). (B) Relationships of sheared quartz (Qz1) with neoformed quartz (Qz2), crosscut by microcracks with bismuthinite (Bit) and electrum (El), (Ferberst vein). (C) Lollingite aggregates (Lo) highly fractured and cemented by hyaline quartz (Qz3) with bismuthinite (Bit) (La-Rode vein). (D) Same picture as (C) in transmitted, polarized light. (E) Lollingite (Lo) crosscut by an assemblage of native bismuth (Bi) and bismuthinite (Bit) (Androl vein). (F) back scattered electron image of the complex Bi-Te assemblage formed in stage 3. Native rounded shape bismuth (Bi) with bismuthinite (Bit) and tetrahedrite (Trt), horobetsuite (Hor) in a hedleyite (Hed) crystal. Ox: unknown oxydes (Ferberst vein).

give the isotopic composition of the initial lead of the dated apatite (Fig. 13C, D). Their composition shows some difference between the Ferbert vein and the Androl vein with respectively  $0.823 \pm 0.005$  and  $0.853 \pm 0.013$ . Those results are consistent with initial  $^{207}\text{Pb}/^{206}\text{Pb}$  ratios measured in different nearby mineralized veins, and main lithological formations of the Brioude-Massiac area (Marcoux and Bril, 1986). Thus, the Fournial (Pb-Ag-Sn-As veins) have  $^{207}\text{Pb}/^{206}\text{Pb}$  ratios different  $0.86234 \pm 0.00027$  ( $n=14$ ), but that of the Sb-(Au) vein of the Céroux is closer  $0.8598 \pm 0.0014$  ( $n=1$ ). On the other Sb-(Au) veins, the isotopic compositions of the lead remain variable within the district. The aplitic dykes close to a leucogranitic composition from the la Margeride pluton, in the southern part of the district, show the strongest correlation with the Androl vein with a  $^{207}\text{Pb}/^{206}\text{Pb}$  ratio of  $0.8569$  ( $n=1$ , composition recalculated at 320 Ma).

## 7 Discussion

### 7.1 Mechanisms of ore-vein formation and chemical-thermal evolution

During stage 1, the initial vein opening, coeval with the massive crystallization of the Qz1 under low-strain, was contemporaneous with a high temperature (up to  $400^\circ\text{C}$ ) paragenesis with wolframite and löllingite from an As and W enriched fluid with low-salinity (about 5 equiv wt% NaCl)  $\text{CO}_2$ - $\text{CH}_4$ -rich  $\pm \text{N}_2$  aqueous fluid (V-type fluid inclusions in the classification of Bril, 1982).

A ductile/brittle deformation episode marks the beginning of stage 2 (Fig. 12). The first Qz1 experienced a dynamic recrystallization shown by undulose extinction, subgrain rotation recrystallization, bulging and quartz neograin (Qz2) formed at the expense of the early Qz1. Ductile/brittle deformation features argue for a deep-seated formation between 12 to 9 km (Scholz, 1988). This is supported by the range of temperature for this stage, estimated around  $480^\circ\text{C}$ , based on the arsenopyrite thermometry and, in agreement with the estimated temperature range ( $400$  to  $500^\circ\text{C}$ ) deduced from the quartz textural observations (e.g. Stipp *et al.*, 2002). Those depth and temperature estimation are in good agreement with the estimated emplacement conditions of the leucogranitic dykes of Bonnac (see Sect. 2.3). The transformations of wolframite into scheelite, and löllingite into arsenopyrite suggest a change in fluid chemistry, still rich in As and W, and marked by an increase in sulfur fugacity and in the calcium activity. The pseudomorphic textures argue for a remobilization of the tungsten from the previous ferberite. The increase of the Ca/Fe ratio in the fluid, associated with a slightly decrease of the temperature, as predicted by Wood and Samson (2000) could possibly correspond to higher fluid interaction with the surrounding metamorphic formations. This fluid could correspond to the L1-type fluid inclusions defined by Bril (1982), with low-salinity (3.5–0 equiv wt% NaCl), lower  $\text{CO}_2$  aqueous fluid, and trapping temperature estimated around  $300$  to  $400^\circ\text{C}$  (Fig. 14).

The onset of stage 3 (Fig. 12) was marked by brittle fracturing. The previous assemblage was micro-brecciated, and invaded by a hyaline, low-strain Quartz (Qz3). This new quartz generation was coeval with the deposition of native bismuth, bismuthinite, hedleyite, electrum, pyrite, and

base-metals minerals (chalcopyrite, sphalerite, galena). The microcrack infill as well as fluid and solid-inclusions bands (Fig. 10A, B) suggest fluid-assisted fracturation under a hydrostatic regime at a depth comprised between 7 and  $<5$  km (Scholz, 1988). This stage 3 might be interpreted as a consequence of a crack-and-seal triggered by a fluid overpressure mechanism (Ramsay, 1980). The emplacement of the previous massive quartz generations could have sealed the porosity in the fault zone and act like an impermeable barrier to fluid flow allowing an increase in the fluid pressure. The crack-and-seal process has triggered pressure drop from lithostatic to hydrostatic regime, and might be interpreted as a consequence of a fault-valve mechanism (Sibson *et al.*, 1988; Cox *et al.*, 1991; Robert *et al.*, 1995; Gaboury and Daigneault, 2000). The textural evolution reflects the transition from a lithostatic pressure context during stages 1 and 2 with a limited permeability to pervasive fluid circulation in connected fractures, therefore implying a transition from, an aseismic to, a seismic environment (Cox, 1987; Cox *et al.*, 1991).

The deposition temperature of gold during stage 3 can be deduced from the paragenetic association of native bismuth and bismuthinite. According to Barton and Skinner (1979), a range of temperature between  $320$  to  $240^\circ\text{C}$  can be proposed. However, the association of native bismuth and hedleyite can only be stable below a temperature of  $266^\circ\text{C}$  (Dimitrova and Kerestedjian, 2006). Therefore, we propose a temperature range between  $266$  to  $240^\circ\text{C}$  for the deposition of stage 3, which is in good agreement with a ca  $200^\circ\text{C}$  homogenization temperature deduced from the L2-type secondary aqueous fluid inclusions (Bril, 1982). This relatively low temperature accounts for the deposition of antimony-rich Bi-Te minerals like the horobetsuite or the tetrahedrite.

### 7.2 Possible mechanisms for gold deposition

The common occurrence of electrum within Bi-Te minerals might emphasize the role of a polymetallic melt/liquid for the concentration of precious metal, as already reported for similar mineralization (Ciobanu *et al.*, 2006; Cook *et al.*, 2007; Ciobanu *et al.*, 2010; Zachariáš *et al.*, 2014). The polyphase character of the ore-inclusions (electrum intergrowth in native bismuth, or electrum, native bismuth intergrowths in hedleyite), the ovoidal shape of the electrum inside native bismuth, and the presence of minerals such as maldonite or horobetsuite might support this mechanism (Ciobanu *et al.*, 2006; Zachariáš *et al.*, 2014). But our deposition temperature estimate, between  $266$  to  $240^\circ\text{C}$ , is too close to, or even below, the bismuth solidus temperature, and the eutectic temperature of the Au-Bi system ( $241^\circ\text{C}$ ). This leads us to suggest that a large part of the gold and Bi-Te phases probably precipitated directly from a hydrothermal fluid enriched in Bi-Te-Au and were not scavenged by a bismuth-rich liquid/melt.

Between stages 1 and 3, a temperature decrease is observed (Fig. 14). In addition, the stage 3 underwent a significant pressure drop associated with a change in tectonic regime, which might have triggered the input of a meteoritic fluid (Bril, 1982; Fig. 14). Furthermore, the decrease in the sulfide activity in the ore-fluid could be responsible for the gold deposition by destabilization of gold-sulfide complexes

**Table 1.** Summary of the EPMA assays obtained on arsenopyrite from the Brioude-Massiac W-As-Bi-Au veins and gold from Bonnac. Estimated temperatures of crystallization with the arsenopyrite geothermometer are compared with the fluid-inclusions data (Bril, 1982).

Arsenopyrite composition	Number of analysis	S (wt%)	Std	Fe	Std	As	Std	Sb	Std	Au	Std	Total	As (at%)	Std	T (°C)	Trapping temperature (°C) estimated by fluid inclusions (Bril, 1982)
Asp from Bonnac W-As-Bi-Au veins (data from this study and Bril, 1983)	60	19.30	0.50	34.40	0.32	45.70	0.68	0.01	0.03	bdl		99.41	33.4	0.66	485	>350
Asp from Vèze W-As-Bi-Au veins (data from Bril, 1983)	3	19.74	0.63	34.87	0.26	45.39	0.89	bdl		bdl		100	32.8	0.87	470	>350
Asp from Bosberly W-As-Bi-Au veins (data from Bril, 1983)	4	19.10	0.46	35.43	0.19	45.47	0.63	bdl		bdl		100	33.0	0.61	480	>350
<b>Gold composition</b>																
Gold from W-As-Bi-Au veins	10	16.7	5.70	82.60	6.92	99.30										

Std: standard deviation; bdl: below detection limit.

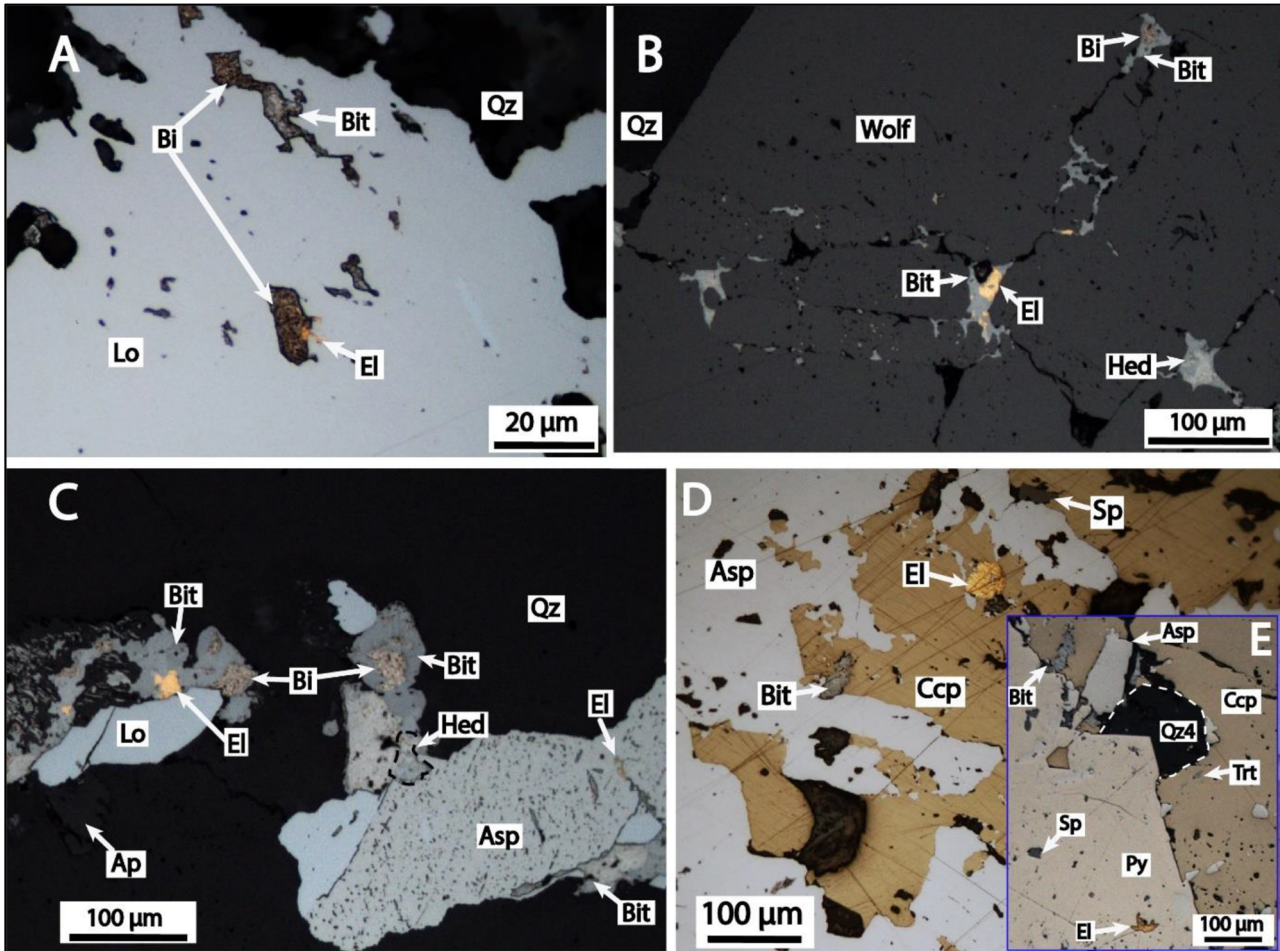


**Fig. 11.** Microphotographs showing gold habits of stage 3 at Bonnac. (A) Lollingite (Lo) with inclusions of electrum (El) within a native bismuth (Bi) – bismuthinite (Bit) patch (Androl vein). (B) Fractured wolframite (Wolf) cemented by bismuthinite (Bit), electrum (El), hedleyite (Hed) and native bismuth (Bi) (Ferbert vein). (C) Residual lollingite (Lo) fractured and cemented by arsenopyrite (Asp) at its turn fractured and cemented by bismuthinite (Bit), electrum (El), hedleyite (Hed) and native bismuth (Bi) (Ferbert vein). (D) Fractured arsenopyrite (Asp) cemented by chalcopyrite (Ccp) with bismuthinite (Bit) inclusions, sphalerite (Sp), electrum (El) (Ferbert vein). (E) Fractured arsenopyrite (Asp) cemented by chalcopyrite (Ccp) with bismuthinite (Bit) inclusions, sphalerite (Sp), tetrahedrite (Trt), euhedral pyrite (Py) contemporaneous with euhedral quartz (Qz4) (Ferbert vein).

associated with the ongoing sulfide precipitation (Williams-Jones *et al.*, 2009).

### 7.3 Tectonic control and timing of ore deposits within the Variscan evolution framework for the French Massif Central

The vein geometry observed in the field is controlled by the inherited structures. The medium dip (30–50°SE) of the Bonnac veins reused the previous fault system coeval with dyke emplacement, whereas the low-angle dip Scoufour veins are controlled by the host-rock foliation. These anisotropy surfaces can be easily reactivated during faulting, and channeled the ore-bearing fluids.

Kinematic data on the striated fault planes coeval with W-As-Bi-Au veins allowed us to derive the stress tensor by an optimized inversion method (Delvaux and Sperner, 2003). The result indicates an extensional tectonic regime with the maximum ( $\sigma_1$ ), intermediate ( $\sigma_2$ ), and minimum ( $\sigma_3$ ) principal

stress axes oriented 39°E/86°, 37°E/04° and 127°E/0°, respectively (Fig. 15). The W-As-Bi-Au quartz veins deposition was controlled by a NW-SE horizontal extension direction, consistent with the NW-SE stretching direction documented for the D4 tectono-magmatic event in the FMC (Faure, 1995). This widespread event, related to the syn-orogenic Variscan extension in the FMC, dated between 325 and 310 Ma, is contemporaneous with the emplacement of the leucogranitic and monzogranitic syn-tectonic plutons (Figs. 1 and 16; Faure and Pons, 1991; Faure, 1995; Faure *et al.*, 2009; Talbot *et al.*, 2005a, 2005b; Joly *et al.*, 2007, 2009).

The hydrothermal apatite grains from two localities in the Bonnac area yield LA-ICP-MS U/Pb dates of  $315.6 \pm 2.8$  for the Ferbert vein (Scoufour area) and  $323.4 \pm 3.2$  Ma for the Androl vein (Bonnac area), respectively interpreted as the emplacement age of the W-As-Bi-Au veins. This age of ca. 320 Ma is consistent with the D4 tectonic, which is also coeval with the Serpukhovian-Bashkirian generation of tungsten ore deposits with minor gold in the FMC as the Puy-les-Vignes or

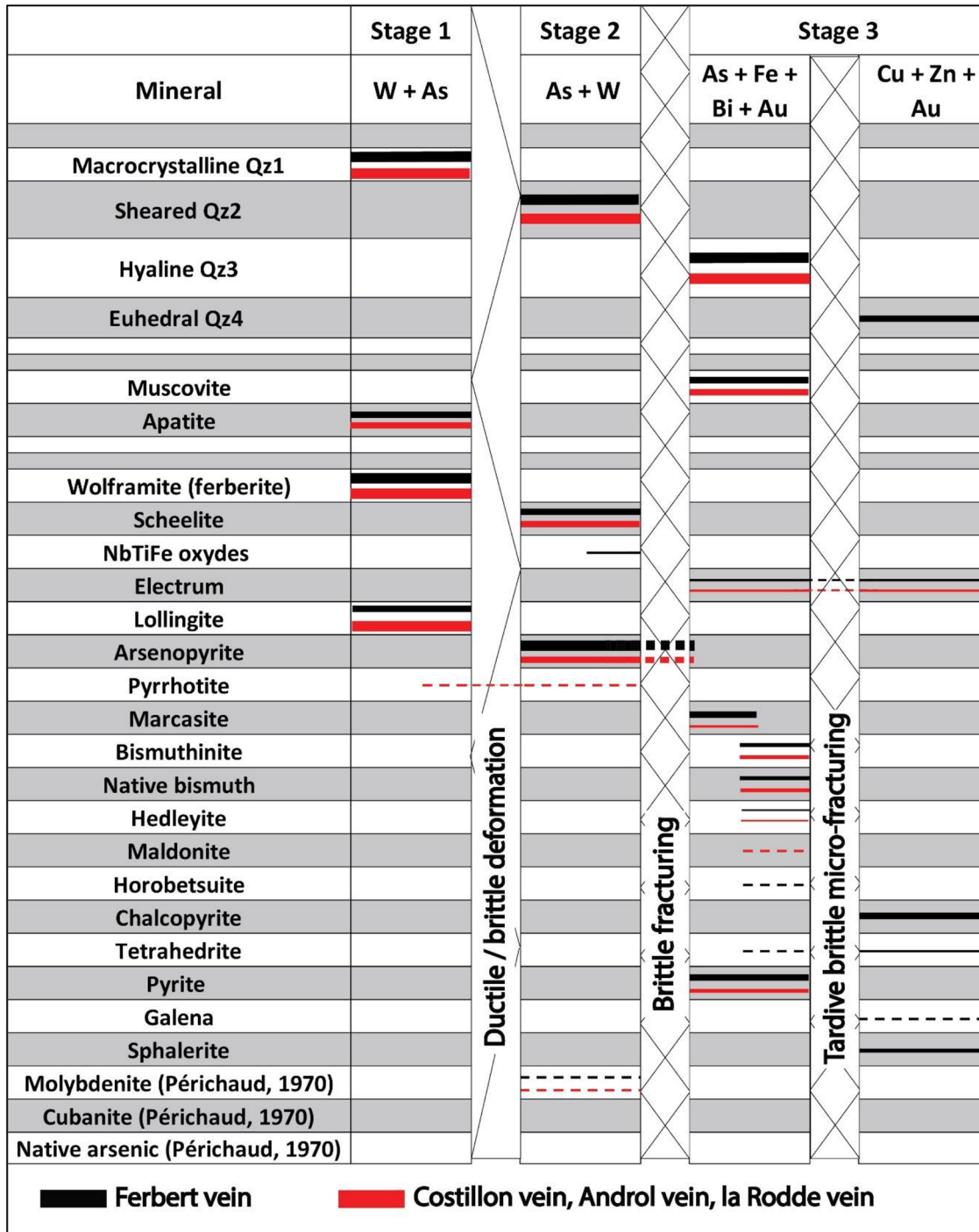
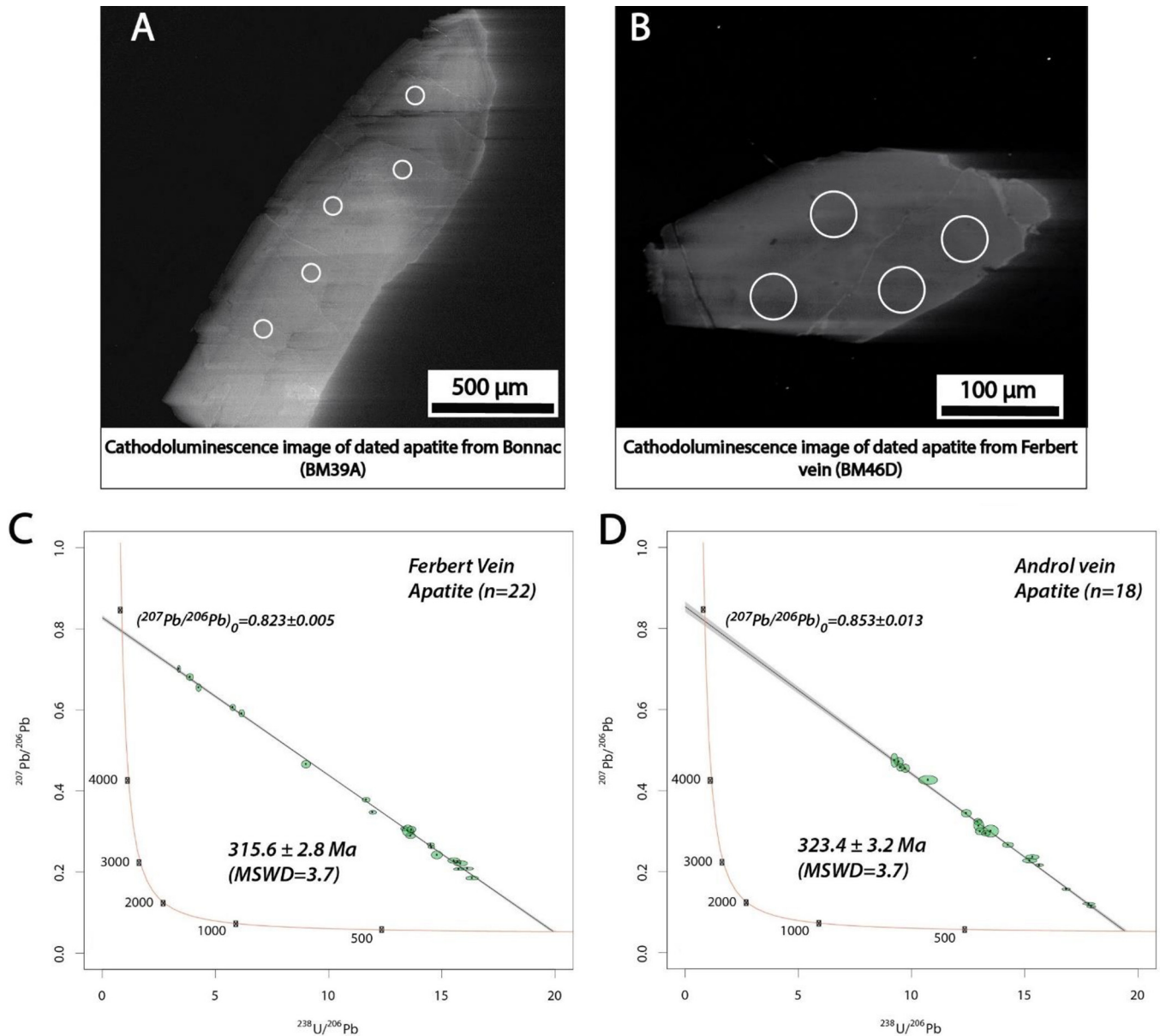


Fig. 12. Paragenetic succession of the Bonnac W-As-Bi-Au mineralization. See text for details.

St-Mélany (Fig. 16; Harlaux *et al.*, 2018). Closer to the Brioude-Massiac district, the Leucamp and Engualès ore deposits in the Châtaigneraie district yielded the most important tungsten resources of the FMC (Derré, 1983; Bogdanoff *et al.*, 1987; Demange *et al.*, 1988; Lerouge and Bouchot, 2009) are other examples of this tungsten ore deposition event.

All previous works (Périchaud, 1970; Bril and Beaufort, 1989) in the Brioude-Massiac district, proposed a single hydrothermal event, responsible for the formation of both

antimony and tungsten-gold from a perigranitic metal zonation. This model seems to be challenged by our results. Despite their spatial link with the antimony veins, the W-As-Bi-Au ones yield a distinct age, since the antimony veins of the Brioude-Massiac district belong to a younger hydrothermal event referred to as the “Or 300” event (Bouchot *et al.*, 2005; Cheval-Garabédian, 2019). We have shown that the Bonnac W-As-Bi-Au mineralizations have a polyphased history in a continuum of time (Fig. 12), which fits with a unique deformation event, decorrelated with the Or300 event.



**Fig. 13.** (A) and (B) Cathodoluminescence images of some of the dated apatite grains from Bonnac (A: Androl vein; B: Ferbert vein). (C) and (D) Tera-Wasserburg concordia diagrams for the hydrothermal apatite from Bonnac. *n* corresponds to the number of apatite grains analyzed. Ellipses and errors are reported at  $2\sigma$ .

The three mineralized stage are all trapped in quartz-veins with same and distinct structural control (D4 tectonic event), same kinematics, a same infilling chronology with a continuity from a ductile/brittle to only-brittle regime, associated with a progressive cooling of the ore-fluid (Figs. 12 and 14), and by the absence of late remobilization textures during the gold stage 3. This, is also attested by the obvious age difference.

Our results, together with the emplacement ages obtained on the gold-bearing quartz veins from the Cévennes district (Chauvet *et al.*, 2012) argue for an earlier Bashkirian-Moscovian gold-hydrothermal event, sometimes associated with tungsten, during the D4 event. Our data allow us to propose a polyphase history in the FMC characterized by two distinct hydrothermal events carrying gold, namely: (i) a first

Serpukhovian to Bashkirian, and (ii) a second, Gzhelian-Asselian, as the Or300 event, that might have re-used the structural discontinuities that controlled the early event. Recent new data obtain on the orogenic-gold deposit of the la Bellière district (Armorican Massif) argue also for a tectonic-hydrothermal gold event earlier than the Or300 event around 340–325 Ma (Cheval-Garabédian *et al.*, 2020).

#### 7.4 Genetic link with the Serpukhovian leucogranites and ore deposit model for the Bonnac area

Based on our results, the genetic relationships between the mineralization and the leucogranitic dykes can also be re-assessed. The leucogranitic dykes from Brioude-Massiac,

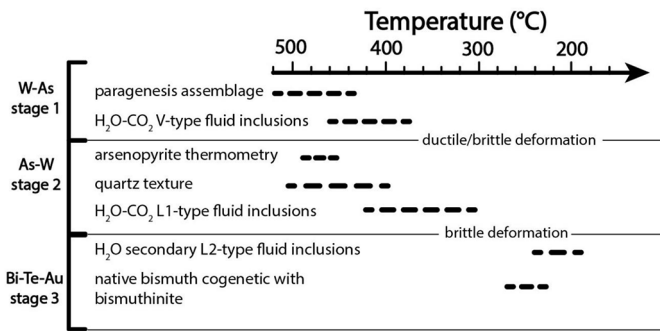


**Fig. 14.** Summary of the evolution of the estimated mineral deposition temperatures for the 3 stages of mineralization of the Bonnac veins, based on all available data. Fluids inclusions data are from [Bril \(1982\)](#), estimated temperature for quartz textural deformation are from [Stipp \*et al.\* \(2002\)](#).

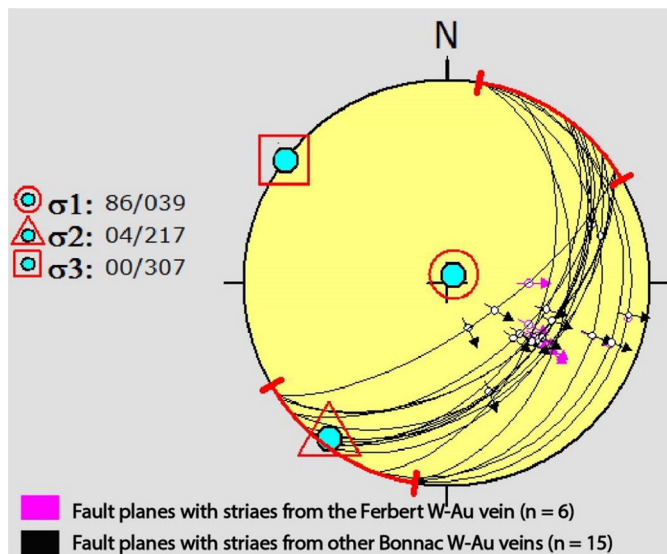


**Fig. 15.** Stereographic projection of faults planes contemporaneous of mineralized quartz veins with their kinematics and associated striae.  $\sigma_1$ ,  $\sigma_2$ ,  $\sigma_3$ : orientation of principal stress axis calculated from fault-slip data inversion using WinTensor software in Schmidt's lower hemisphere equal-area projection ([Delvaux and Sperner, 2003](#)).

dated at  $322 \pm 7$  Ma ([Bril \*et al.\*, 1991](#)) were emplaced contemporaneously with the D4 event and are spatially related to the W-As-Bi-Au deposits. The mineralizing event that followed the intrusive rocks emplacement could be interpreted as a magmatic-to-hydrothermal evolution ([Fig. 17](#); [Linnen and Cuney, 2005](#); [Gloaguen, 2006](#)) with a relatively long-time duration, around 329–316 Ma (dating of the leucogranitic magmatic event). Several lines of evidence support this interpretation as:

- the spatial and temporal link between dykes and mineralized veins;
- their formation during the D4 tectonic event;
- the high temperature paragenesis of stage 1 at 400–500 °C, close to the 600–650 °C emplacement temperature estimated for the andalusite-leucogranitic dykes;

- their close emplacement depths estimated around 10 km ([Sandras, 1988](#));
- the reworking of previous structural discontinuities.

Throughout the Variscan Orogen, there are examples of W-Au deposits that were emplaced within a time gap of ca. 10 Ma after the intrusions of peraluminous magmas ([Romer and Kroner, 2016](#)). In France, the Puy-les-Vignes deposit ([Harlaux \*et al.\*, 2018](#)), and the Salau deposit in the French Pyrenees ([Poitrenaud \*et al.\*, 2019](#)), or in the Bohemian Massif, the Mokrsko deposit ([Zachariáš \*et al.\*, 2014](#)), are good examples of this relation.

A two-stage evolutive model for the magmatic-hydrothermal system in the Bonnac area is proposed in a continuum of time ([Fig. 17](#)). Between 329 and 315 Ma, the emplacement of leucogranitic dykes, related to an underlying pluton, was controlled by normal faulting in the regional NW-SE extensional regime. Slightly younger from the dyke crystallizations, between 321 to 316 Ma, the deformation became more localized and contemporaneous with quartz veins emplacement that recorded a magmatic-to-hydrothermal transition ([Fig. 17](#), stage 2). These hydrothermal fluids have reused the previous discontinuities as feeder channels.

The metamorphic or magmatic origin of the ore-forming fluid for peri-granitic ore deposits is still a matter of debate ([Lang and Baker, 2001](#); [Boiron \*et al.\*, 2001](#); [Hart \*et al.\*, 2002](#); [Bouchot \*et al.\*, 2005](#); [Hart, 2007](#); [Zachariáš \*et al.\*, 2014](#); [Marcoux \*et al.\*, 2015](#)). In the Bonnac area, the magmatic origin of the fluid is not fully demonstrated by the existing fluid inclusion study ([Bril, 1982](#)) as they rather display a metamorphic origin (low salinity, complex chemistry enriched in  $\text{CO}_2$ ). However, a magmatic fluid affinity is pointed out by: (i) the presence of magmatic affinity element such as the W and the Bi-Te-Au association ([Lang and Backer, 2001](#); [Blevin, 2004](#)) and by (ii) the spatial and temporal link with leucogranitic dykes. In addition, the lead isotopic compositions measured for different mineralized veins and main lithological formations of the Brioude-Massiac area support such magmatic origin of the metals ([Marcoux and Bril, 1986](#)). The  $^{207}\text{Pb}/^{206}\text{Pb}$  ratios estimated on our dating are close to those obtained on the aplitic dykes of leucogranitic composition of the la Margeride granite (see [Sect. 6](#) for the data).

To take into account all those features, we propose a genetic link between those mineralized veins and the leucogranitic dykes, where the initial magmatic fluids were derived from the crystallization of an underlying granitic pluton. The heat source supplied by the pluton was responsible for fluid migration toward the high permeability zones. The high temperature (400–500 °C) interaction between the fluid and the host-rocks (greisen type alteration in the vein hanging walls) could have re-equilibrated the fluid, overprinting its initial magmatic signature. Then fault-valve mechanisms channeled the ore-fluids into structural discontinuities ([Sibson \*et al.\*, 1988](#)), and fluid overpressure associated with potential fault-valve mechanism could be responsible for vein opening and the gold-stage 3 deposition, in a shallow crustal environment.

The chemical composition of the Brioude-Massiac andalusite-leucogranitic S-type magma dykes (EDM 1) is characterized by an oxidizing redox state ([Fig. 18](#)), although a

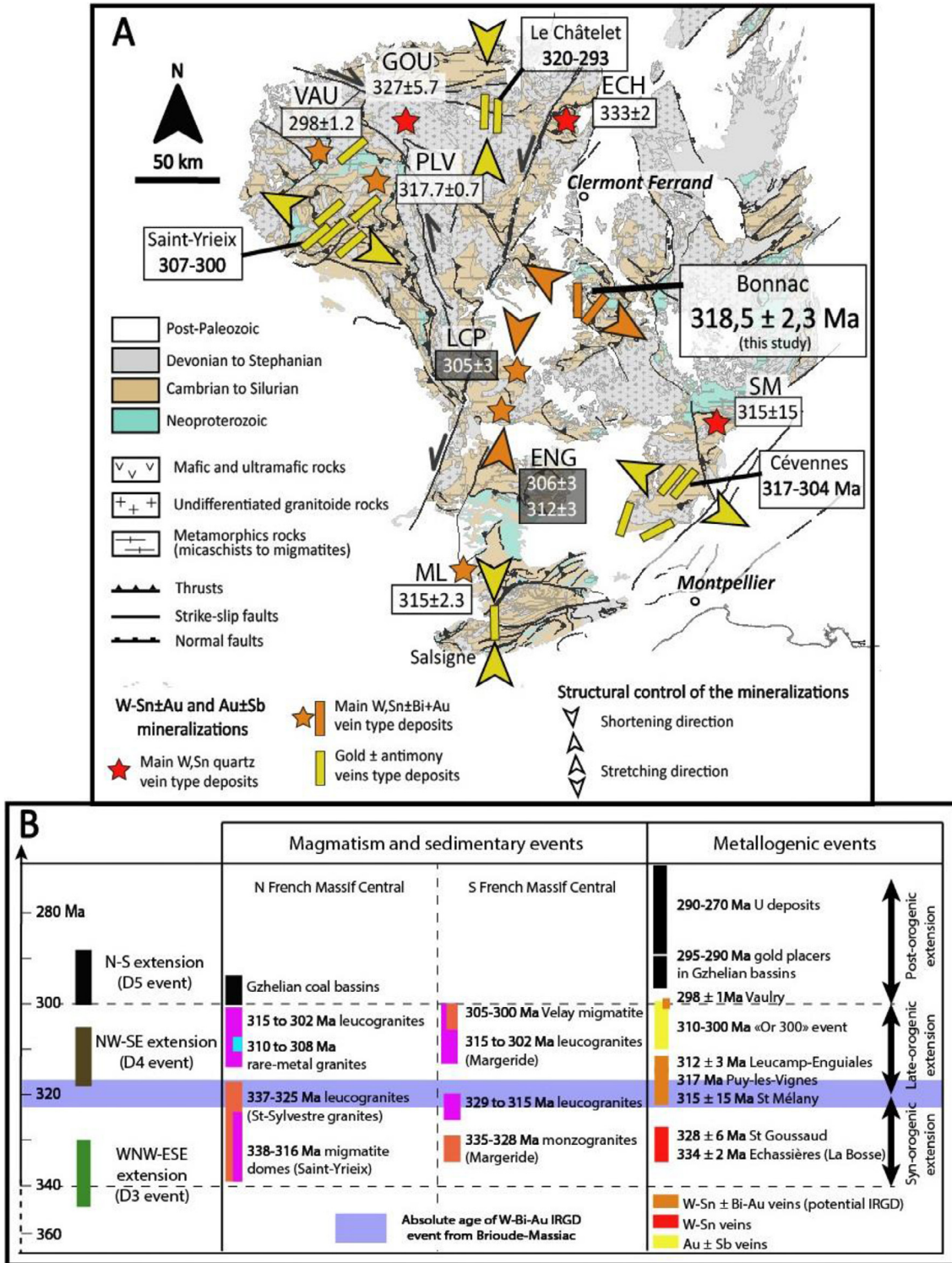


**Fig. 16.** (A) Synthesis of the structural control and radiometric age compilation of orogenic gold ± antimony district, W-Sn and W-Bi-Au vein-type districts (Béziat *et al.*, 1980; Bouchot *et al.*, 2005; Harlaux *et al.*, 2018). White boxes correspond to U-Pb dating on wolframite by TIMS method, from Harlaux *et al.* (2018). Black boxes correspond to Ar/Ar dating on muscovite from Monié *et al.* (1999, 2000). For the orogenic-gold deposits, le Châtelet dating (K/Ar on illites) is from Bouchot *et al.* (2005); from Nicaud (2001) for Saint-Yrieix district (K/Ar on illite); from Chauvet *et al.* (2012) for the Cévennes district (Ar/Ar on muscovite). District name abbreviations are the same as in Figure 1. Geological map modified after Chantraine *et al.* (1996). (B) The Bonnac hydrothermal event is replaced in the different geodynamic events of the Variscan orogen in the French Massif Central (Faure *et al.*, 2009).

reduce redox state is more commonly observed. These characteristics are considered as more favorable than a reduce redox state to form a tungsten ore deposit. Indeed the early magnetite precipitation allows the preservation of Au in the melt fraction of granitic magmas (Blevin, 2004).

## 7.5 New ore deposit model for the Bonnac deposits?

Because of the metamorphic origin of fluids, the Bonnac deposits was previously classified as an orogenic gold deposit (Bouchot *et al.*, 2005), although they do not fulfill all the necessary criteria (Groves *et al.*, 1998).

The Bonnac deposits share some of the characteristics of the IRGD type (Thompson *et al.*, 1999; Lang and Baker, 2001; Hart *et al.*, 2002; Gloaguen, 2006; Hart, 2007; Zachariáš *et al.*, 2014; Marcoux *et al.*, 2015) such as:

- the spatial and temporal relationships between ore-deposition and peraluminous granite emplacement;
- the peculiar relation between magmatic-source-related ore phases such as bismuth, tellurides, wolframite, löllingite or molybdenite;
- the contemporaneous bismuth-telluride-gold deposition;
- the vein deposition during the syn-orogenic extensional period.

The redox state of the leucogranitic dykes that spans the boundary of the ilmenite series (Fig. 18) is also a favorable context for IRGD deposits (Lang and Baker, 2001; Blevin, 2004).

On the other hand, the structural evolution from a ductile/brittle deformation to a brittle one, fault-valve mechanism features, and the presence of a late meteoric fluid input, are classical features found for the orogenic gold type deposits (Boiron *et al.*, 1990, 2003; Groves *et al.*, 1998; Bouchot *et al.*, 2005).

Therefore, the Bonnac ore-zone represents a mineralization type intermediate between the orogenic-gold and IRGD models as already demonstrated for the Mokrsko gold deposit in the Bohemian-Massif for example (Zachariáš *et al.*, 2014).

## 8 Conclusions

The Bonnac veins show a W-As-Bi-Au paragenesis that results from polyphase hydrothermal and magmatic events. Three stages of ore deposition have been identified starting with wolframite and löllingite in a deep-seated setting, between 12 to 9 km and up to 400 °C. The second ductile/brittle deformation stage was responsible for scheelite and arsenopyrite deposition at 480–300 °C. The late stage was marked by brittle micro-fracturing infilled with native bismuth, bismuthinite, hedleyite, electrum, pyrite and Cu-Zn-Pb minerals at 266 to 240 °C and 7 to <5 km depth. This could be the result of fault-valve mechanism. The decrease of the temperature-pressure and the sulfide activity caused by ongoing sulfide precipitation seems to be the major factors responsible for the gold deposition during the late stage of deposition.

The mineralized veins are spatially and temporally linked to the emplacement of the andalusite-leucogranitic dykes of the Brioude-Massiac district around 329–315 Ma. Our new

LA-ICP-MS U/Pb dating on hydrothermal apatite from the deposit documents an emplacement age around 320 Ma. This genetic link suggests a magmatic-to-hydrothermal transition for the Bonnac ore-forming process. In the newly proposed model, the cooling of a peraluminous pluton might have supplied magmatic fluids, and heat source for mineralized fluid flows toward high permeability zones such as previous discontinuities. The magmatic origin of the fluid has been partly overprinted by fluid-rocks interaction.

The emplacement of both the andalusite-leucogranitic dykes and quartz veins was controlled at the regional scale by a NW-SE extensional direction, consistent with the tectono-magmatic D4 event corresponding to the syn-orogenic extension in the FMC Variscan orogen. This geodynamic event is older than the “Or 300” one, suggesting therefore an earlier fertile metallogenic period at ca. 320 Ma for tungsten and gold deposition in the FMC.

The genetic classification of the Bonnac mineralization is equivocal. The W-As-Bi-Au-quartz veins exhibit the features of both orogenic gold (relatively deep level of emplacement) and IRGD model (spatial-temporal link between the mineralization and the peraluminous intrusion). We propose that it represents an intermediate type between the typical orogenic-gold and IRGD model.

The Serpukhovian to Bashkirian peraluminous andalusite-leucogranitic dyke swarms appear as a favorable metallotect for future mining exploration in the FMC. The widespread occurrences related to this type of magmatism in the FMC suggest that other Bonnac-like, or IRGD-like, deposits probably exist. IRGD deposits, and the economic high-grade gold content in tungsten vein-type, might have been underestimated in the FMC.

## Supplementary material

*ESM1*: Geochemical compositions of the Brioude-Massiac leucogranitic dykes replaced in the A) A-B plot, and B) Q-P plot from Debon and Le Fort (1988) diagrams. Data from Sandras (1988).

*ESM2*: Electron microprobe analyses of arsenopyrite and the gold grain from the Bonnac veins.

*ESM3*: Operating conditions for the LA-ICP-MS equipment and LA-ICP-MS U/Pb analyses for the apatites from the studied samples.

The supplementary material is available at <https://www.bsgf.fr/10.1051/bsgf/2020041/olm>.

*Acknowledgements.* This work was funded by e-Mines Company through its R&D activity, and the ISTO with contribution from ANRT. The authors thank the following persons for their technical support and valuable advices: T. Poitrenaud, B. Cochelin, A. Beaudoin, R. Augier, C. Montmartin, J. Gouin, M. Picault. We particularly thank I. Di-Carlo (ISTO) for the SEM, cathodoluminescence and microprobe analyses and for valuable advices. S. Janiec, G. Badin, and P. Benoist-Julliot (ISTO) for thin sections preparation, and technical assistance, and the GeOHeLiS platform for the LA-ICP-MS dating. We also gratefully acknowledge Pr. L. Jolivet and Dr. O. Vanderhaeghe, for their efficient editorial handling, and Pr. D. Béziat and one anonymous reviewer for their constructive comments that improved this manuscript significantly.

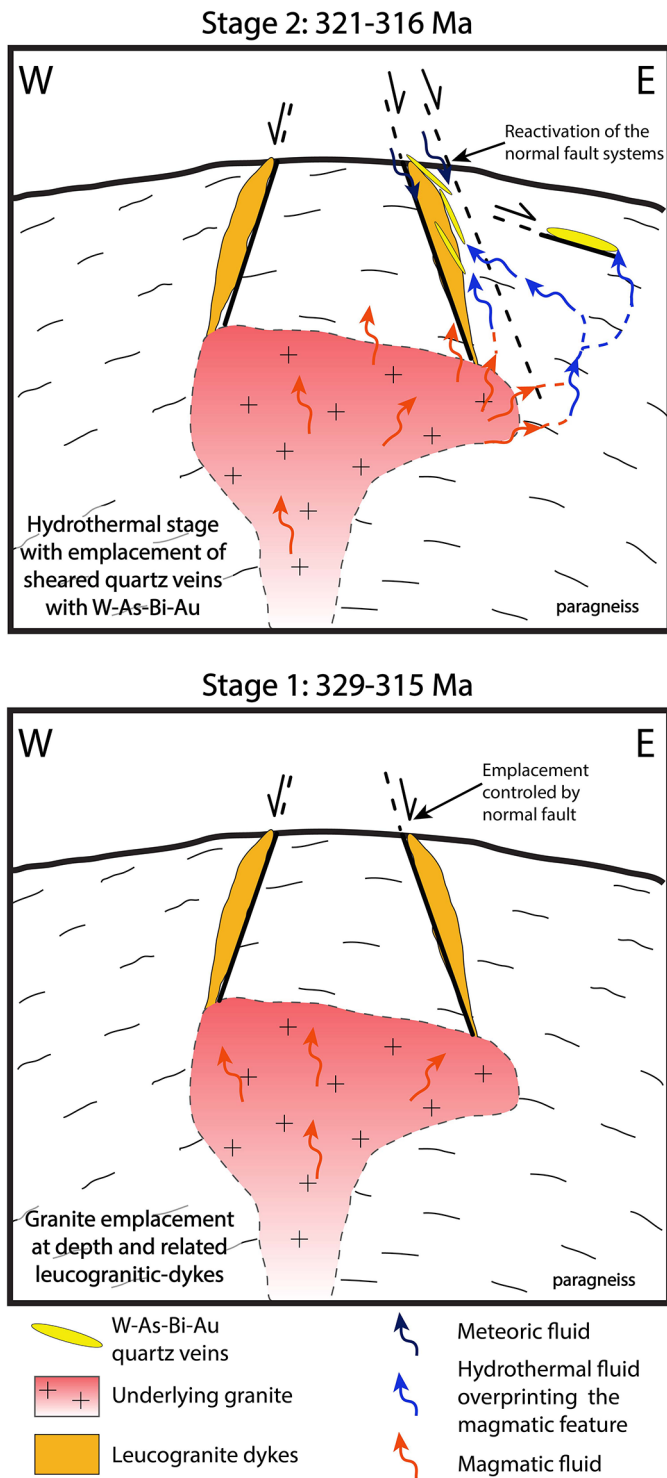


**Fig. 17.** Metallogenic model of the Bonnac W-Bi-Au quartz veins system (not to scale).

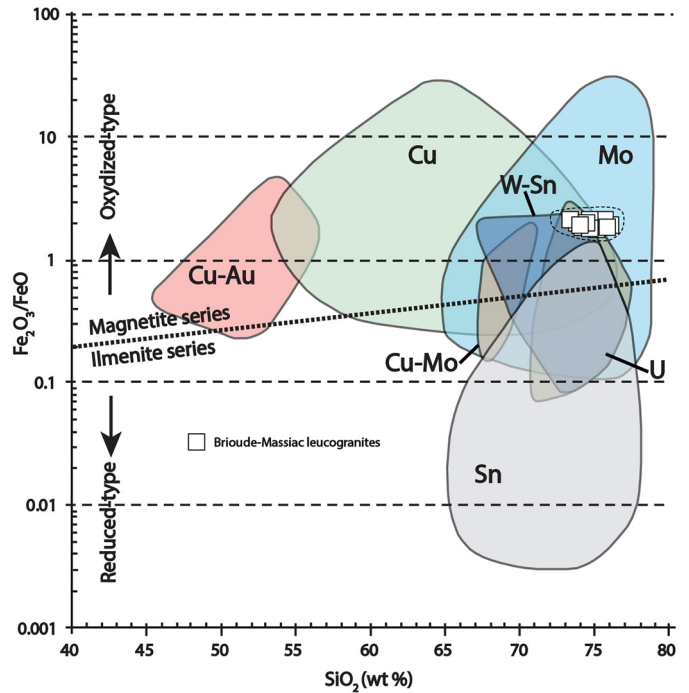


**Fig. 18.** Fe<sub>2</sub>O<sub>3</sub>/FeO versus SiO<sub>2</sub> diagram for granitoid rocks associated with various mineral deposits, compiled from Harlaux *et al.* (2018). Data from the leucogranites dykes of the Brioude-Massiac district are from Sandras (1988).

## References

- Audion AS, Labbé JF. 2012. Panorama mondial 2011 du marché du tungstène. Rapport Public BRGM, RP-61341-FR, 108 p.
- Barton PB, Skinner BJ. 1979. Sulfide mineral stabilities. In: Barnes HL, ed. *Geochemistry of hydrothermal ore deposits*. New York: John Wiley, pp. 278–403.
- Bernard-Griffiths J, Lasnier B, Marchand J, Vidal P. 1980. Approche par la méthode Rb/Sr de l'étude de granulites acides en Haut-Allier (Massif Central français). *Réun Ann Sci Terre* 8: 41 p.
- Béziat P, Prouhet JP, Tollon F. 1980. Le district de Montredon-Labessonnié (Tarn): W, Sn, F. Publications du 26e Congrès Géologique International (Paris). *Gisements français* 7: 42 p.
- Bogdanoff S, Cirodde JL, Ploquin A, Ramboz C, Le Chapelain JR, Mignon R. 1987. Exploration for tungsten in the Châtaigneraie district. *Chron Rech Min* 487: 11–30.
- Blevin PL. 2004. Redox and compositional parameters for interpreting the granitoid metallogeny of eastern Australia: implications for gold-rich ore systems. *Resource Geology* 54: 241–252.
- Boiron MC, Cathelineau M, Dubessy J, Bastoul AM. 1990. Fluids in Hercynian Au veins of from the French Variscan belt. *Mineralogical Magazine* 54: 231–243.
- Boiron MC, Barakat A, Cathelineau M, Banks DA, Durisova J, Moravek P. 2001. Geometry and P-V-T-X conditions of

- microfissural ore fluid migration: the Mokrsko gold deposit (Bohemia). *Chem Geol* 173: 207–225.
- Boiron MC, Cathelineau M, Banks DA, Fourcade S, Vallance J. 2003. Mixing of metamorphic and surficial fluids during the uplift of the Hercynian upper crust: consequences for gold deposition. *Chem Geol* 194: 119–141.
- Bouchot V, Ledru P, Lerouge C, Lescuyer J-L, Milesi J-P. 2005. Late Variscan mineralizing systems related to orogenic processes: the French Massif Central. *Ore Geol Rev* 27: 169–197.
- Bril H. 1982. Fluid inclusions study of Sn-W-Au, Sb- and Pb-Zn mineralizations from the Brioude-Massiac district (French Massif Central). *Tschermaks Min Petr Mitt* 30: 1–16.
- Bril H. 1983. Étude métallogénique des minéralisations à antimoine et associées du district de Brioude-Massiac (Massif Central français); conditions géochimiques de dépôt, implications génétiques, PhD thesis. Université Clermont-Ferrand, 341 p.
- Bril H, Beaufort D. 1989. Hydrothermal alteration and fluid circulation related to W, Au, and Sb vein mineralizations, Haut-Allier, Massif Central, France. *Econ Geol* 84: 2237–2251.
- Bril H, Bonhomme MG, Marcoux E, Baubron JC. 1991. Ages K/Ar des minéralisations de Brioude-Massiac (W-Au-As-Sb; Pb-Zn), Pontgibaud (Pb-Ag; Sn), et Labesette (As-Pb-Sb-Au): place de ces districts dans l'évolution géotectonique du Massif Central français. *Miner Depos* 26: 189–198.
- Burg J-P, Matte P. 1978. A cross section through the French Massif Central and the scope of its Variscan geodynamic evolution. *Z dt Geol Ges* 129: 429–460.
- Chantraine J, Autran A, Cavellier C. 1996. Geological map of France, 1/1 000 000. Orléans: BRGM.
- Charonnat X. 2000. Les minéralisations aurifères tardi-hercyniennes des Cévennes, PhD thesis. Université d'Orléans, 1 vol, 259 p.
- Chauvet A, Volland-Tuduri N, Lerouge C, *et al.* 2012. Geochronological and geochemical characterization of magmatic-hydrothermal events within the Southern Variscan external domain (Cévennes area, France). *Int J Earth Sci* 101: 69–86.
- Cheval-Garabédian F. 2019. Les minéralisations à Sb et Au tardi-varisques: vers un modèle génétique unifié? Exemples du Massif armoricain et du Massif central, PhD thesis. Université d'Orléans, 1 vol, 498 p.
- Cheval-Garabédian F, Faure M, Marcoux E, Gouin J, Picault M. 2020. The La Bellière gold and antimony district (French Armorican Massif): a two-stage evolution model controlled by Variscan strike-slip tectonic. *Ore Geol Rev* 125: 103–681.
- Ciobanu CL, Cook NJ, Damian F, Damian G. 2006. Gold scavenged by bismuth melts: an example from Alpine shear-remobilizations in the Highis Massif Romania. *Miner Petrol* 87: 351–384.
- Ciobanu CL, Birch WD, Cook NJ, Pring A, Grundler PV. 2010. Petrogenetic significance of Au–Bi–Te–S associations: the example of Maldon, Central Victorian gold province, Australia. *Lithos* 116: 1–17.
- Cook NJ, Ciobanu CL, Wagner T, Stanley CJ. 2007. Minerals of the system Bi–Te–Se–S related to the tetradymite archetype: review of classification and compositional variation. *Can Miner* 45: 665–708.
- Cox SF. 1987. Antitaxial crack-seal vein microstructures and their relationships to displacement paths. *J Struct Geol* 9: 79–787.
- Cox SF, Wall VJ, Etheridge MA, Potter TF. 1991. Deformation and metamorphic processes in the formation of mesothermal vein-hosted gold deposits, examples from the Lachlan Fold Belt in central Victoria Australia. *Ore Geol Rev* 6: 391–423.
- Cuney M, Alexandrov P, Le Carlier de Veslud C, *et al.* 2002. The timing of W Sn rare metals mineral deposit formation in the Western Variscan chain in their orogenic setting: the case of the Limousin area (Massif Central, France). In: Blundell DJ, Neubauer F, von Quadt A, eds. The timing and location of major ore deposits in an evolving Orogen. *Geological Society, London, Special Publications* 204: 213–228.
- De Gramont X, Feybesse JL, Lambert A. 1990. Synthèse du district de Brioude-Massiac et des confins nord de la Margeride (Massif Central). Rapport BRGM DAM/DL/C/R-30695, 191 p.
- Delvaux D, Sperner B. 2003. Stress tensor inversion from fault kinematic indicators and focal mechanism data: the TENSOR program. *New Insights into Structural Interpretation and Modelling* 212: 75–100.
- Demange M, Nicolas V-A, Soler P, Giouse H. 1988. Le gisement tungstifère de Leucamp (Cantal, France). Contrôles géologiques et minéralisations. *Bull Soc Géol Fr* 4: 559–570.
- Derré C. 1983. La province à Sn-W ouest-européenne. Histoire de divers types de gisements du Massif Central, des Pyrénées et du Portugal. Distributions des gisements, PhD thesis. Université Paris VI, 2 vol., I, 345 p., II, 421 p.
- Dimitrova D, Kerestedjian T. 2006. Bismuth minerals in the postskarn sulphide-arsenide mineralization in the Martinovo iron deposit, NW Bulgaria. *Geochemistry, Mineralogy and Petrology, Sofia* 44: 19–32.
- Faure M. 1995. Late orogenic carboniferous extensions in the Variscan French Massif Central. *Tectonics* 14: 132–153.
- Faure M, Pons J. 1991. Crustal thinning recorded by the shape of the Namurian-Westphalian leucogranites in the Variscan belt of the Northwest Massif Central, France. *Geology* 19: 730–733.
- Faure M, Be Mézème E, Duguet M, Cartier C, Talbot J-Y. 2005. Paleozoic tectonic evolution of medio-Europa from the example of the French Massif Central and Massif Armorican. In: Carosi R, Dias R, Iacopini D, Rosenbaum G, eds. The southern Variscan belt. *Journal of the Virtual Explorer* 19 (Electronic Edition, ISSN 1441-8142).
- Faure M, Lardeaux J-M, Ledru P. 2009. A review of the pre-Permian geology of the Variscan French Massif central. *Comptes Rendus Geoscience* 341: 202–213.
- Gaboury D, Daigneault R. 2000. Flat vein formation in a transitional crustal setting by self-induced fluid pressure equilibrium, an example from the Géant Dormant gold mine Canada. *Ore Geol Rev* 17: 155–178.
- Gloaguen E. 2006. Apport d'une étude intégrée sur les relations entre granite et minéralisations filoniennes (Au et Sn-W) en contexte tardi-orogénique, PhD thesis. Université d'Orléans.
- Groves DI, Goldfarb RJ, Gebre-Mariam M, Hagemann SG, Robert F. 1998. Orogenic gold deposits, a proposed classification in the context of their crustal distribution and relationship to other gold deposit types. *Ore Geol Rev* 13: 7–27.
- Harlaux M, Marignac C, Cuney M, Mercadier J, Magott R, Mouthier B. 2015. Nb-Ti-Y-HREE-WU oxide minerals with uncommon compositions associated with the tungsten mineralization in the Puy-les-Vignes deposit (Massif central, France): evidence for rare-metal mobilization by late hydrothermal fluids with a peralkaline signature. *Can Miner* 53: 653–672.
- Harlaux M, Romer RL, Mercadier J, Morlot C, Marignac C, Cuney M. 2018. 40 Ma of hydrothermal W mineralization during the Variscan orogenic evolution of the French Massif Central revealed by U-Pb dating of wolframite. *Miner Depos* 53: 21–51.
- Hart CJR, McCoy D, Goldfarb RJ, *et al.* 2002. Geology, exploration and discovery of the Tintina gold province, Alaska and Yukon. *Society of Economic Geologists Special Publication* 9: 241–274.
- Hart CJ. 2007. Reduced intrusion-related gold systems. *Geological Association of Canada, Mineral Deposits Division* 5: 95–112.

- Joly A, Chen Y, Faure M, Martelet G. 2007. Multidisciplinary study of a syntectonic pluton close to a major lithospheric-scale fault: relationships between the Montmarault granitic massif and the Sillon Houiller Fault in the Variscan French Massif Central. Part I: geochronology, mineral fabrics and tectonic implications. *J Geophys Res* 112: B10104.
- Joly A, Faure M, Chen Y, Martelet G. 2009. Gravity inversion, AMS and geochronological investigations of syntectonic granitic plutons in the southern part of the Variscan French Massif Central. *J Struct Geol* 31: 421–443.
- Kretschmar U, Scott SD. 1976. Phase relations involving arsenopyrite in the system Fe-As-S and their application. *Can Miner* 14: 364–386.
- Lang J-R, Baker T. 2001. Intrusion related gold systems: the present level of understanding. *Miner Depos* 36: 477–489.
- Lasnier B. 1977. Persistance d'une série granulitique au cœur du Massif central français (Haut Allier). Les termes basiques, ultrabasiques et carbonatés, PhD. Thesis. Université de Nantes, 341 p.
- Lasnier B, Marchand J, Bouilkler R, Burg J-P, Cornen G, Forestier FH, *et al.* 1982. Notice de la carte géologique de France (1/50 000), feuille de Brioude (766). Orléans: BRGM.
- Ledru P, Lardeaux JM, Santallier DA, *et al.* 1989. Où sont les nappes dans le Massif central français? *Bulletin de la Société géologique de France* 3: 605–618.
- Lerouge C, Bouchot V. 2009. Conditions of formation and origin of fluids of quartz-tourmaline veins in the La Châtaigneraie tungstiferous district (Massif Central, France) : fluid inclusions and stable isotopes. *Bull Soc Geol Fr* 180: 263–270.
- Linnen RL, Cuney M. 2005. Granite-related rare-element deposits and experimental constraints on Ta-Nb-W-Sn-Zr-Hf mineralization. In: Linnen RL, Samson IM, eds. Rare-element geochemistry and mineral deposits. *Geological Association of Canada, GAC Short Course Notes* 17: 45–68.
- Malavieille J, Guihot P, Costa S, Lardeaux JM, Gardien V. 1990. Collapse of the thickened Variscan crust in the French Massif Central: Mont Pilat extensional shear zone and St. -Étienne Late Carboniferous basin. *Tectonophysics* 177: 139–149.
- Marchand J. 1974. Persistance d'une série granulitique au cœur du Massif central français (Haut Allier). Les termes acides, PhD. Thesis. Université de Nantes, 267 p.
- Marcoux E, Picot P. 1985. Les minéralisations de Pontgibaud (Puy-de-Dôme) : une approche complémentaire par géochimie isotopique du plomb et les paragenèses. *Chronique de la Recherche Minière* 481: 27–38.
- Marcoux E, Bril H. 1986. Héritage et sources de métaux d'après la géochimie isotopique du plomb; étude des minéralisations filoniennes du Haut-Allier (Massif Central, France). *Miner Depos* 21: 35–43.
- Marcoux E, Bonnemaïson M. 1988. La géochimie isotopique du plomb et la prospection de l'or en France. In: Johan Z, Newstetter D, eds. Gisements métallifères dans leur contexte géologique. *Doc BRGM* 158: 489–508.
- Marcoux E, Nerci K, Branquet Y, *et al.* 2015. Late-Hercynian Intrusion-related gold deposits: an integrated model on the Tighza polymetallic district, central Morocco. *Journal of African Earth Sciences* 107: 65–88.
- Marignac C, Cuney M. 1999. Ore deposits of the French Massif Central: insight into the metallogenesis of the Variscan collision belt. *Miner Depos* 34: 472–504.
- Mathonnat M. 1983. La série métamorphique du Cézallier, Massif central français, PhD thesis. Université de Clermont-Ferrand.
- Monié P, Bouchot V, Faure M, Charonnat X, Najoui K. 1999. <sup>40</sup>Ar/<sup>39</sup>Ar Laser-Probe Dating of W, Au and/or Sb Deposits and associated granites in the Southern French Massif Central (Cévennes, Châtaigneraie), EUG 10, abstract volume. Strasbourg: Terra Abstracts, p. 477.
- Monié P, Respaut J-P, Brichaud S, Bouchot V, Faure M, Roig J-Y. 2000. <sup>40</sup>Ar/<sup>39</sup>Ar and U-Pb geochronology applied to Au-W-Sb metallogenesis in the Cévennes and Châtaigneraie districts (Southern Massif Central, France). In: Bouchot V, Moritz R, eds. A Geode-GéoFrance 3D Workshop on Orogenic Gold Deposits in Europe with Emphasis on the Variscides; Extended Abstracts. *Documents du BRGM* 297: 77–79.
- Morisson GW, Rose WJ, Jaireth S. 1991. Geological and geochemical controls on the silver content (fineness) of gold in gold-silver deposits. *Ore Geol Rev* 6: 333–364.
- Nicaud J. 2001. Contrôle structural de la mise en place des minéralisations aurifères du district de Saint-Yrieix : analyse de la fracturation, étude des altérations hydrothermales, PhD thesis. Université de Limoges, 252 p.
- Paquette JL, Piro JL, Devidal J-L, *et al.* 2014. Sensitivity enhancement in LA-ICP-MS by N<sub>2</sub> addition to carrier gas: application to radiometric dating of U-Th-bearing minerals. *Agilent ICP-MS J* 58: 4–5.
- Périchaud JJ. 1970. Les gisements métalliques du district d'antimoine de Brioude-Massiac (Massif central français), PhD thesis. Université de Clermont Ferrand, 771 p.
- Pin C, Peucat J-J. 1986. Ages des épisodes de métamorphisme paléozoïques dans le Massif central et le Massif armoricain. *Bull Soc Géol France* 8, t. II(3): 461–469.
- Pochon A, Gapais D, Gloaguen E, *et al.* 2016. Antimony deposits in the Variscan Armorican belt, a link with mafic intrusives? *Terra Nova* 28: 138–145. <https://doi.org/10.1111/ter.12201>.
- Poitrenaud T, Poujol M, Augier R, Marcoux E. 2019. The polyphase evolution of a late Variscan W/Au deposit (Salau, French Pyrenees): insights from REE and U/Pb LA-ICP-MS analyses. *Miner Depos*: 1–21.
- Ramsay JG. 1980. The crack-seal mechanism of rock deformation. *Nature* 284: 135–139.
- Robert F, Boullier AM, Firdaus K. 1995. Gold-quartz veins in metamorphic terranes and their bearing on the role of fluids in faulting. *J Geophys Res* 100: 12841–12859.
- Romer RL, Kroner U. 2016. Phanerozoic tin and tungsten mineralization—tectonic controls on the distribution of enriched protoliths and heat sources for crustal melting. *Gondwana Res* 31: 60–95.
- Sandras A. 1988. Les structures auro-antimonifères du district de Brioude-Massiac. Gîtologie et métallogénie des concentrations aurifères, PhD thesis. Université de Nancy, 211 p.
- Scaillet S, Cheilletz A, Cuney M, Farrar E, Archibald DA. 1996. Cooling pattern and mineralization history of the saint Sylvestre and western Marche leucogranite pluton, French massif central: I. <sup>40</sup>Ar/<sup>39</sup>Ar isotopic constraints. *Geochim Cosmochim Acta* 60: 4653–4671.
- Scholz CH. 1988. The brittle-plastic transition and the depth of seismic faulting. *Geologische Rundschau* 77: 319–328.
- Sibson RH, Robert F, Poulsen KH. 1988. High-angle reverse faults, fluid pressure cycling, and mesothermal gold-quartz deposits. *Geology* 16: 551–555.
- Sharp ZD, Essene EJ, Kelly WC. 1985. A re-examination of the arsenopyrite geothermometer; pressure considerations and applications to natural assemblages. *Can Miner* 23: 517–534.
- Stipp M, Stünitz H, Heilbronner R, Schmid SM. 2002. The eastern Tonale fault zone: a natural laboratory for crystal plastic deformation of quartz over a temperature range from 250 to 700 °C. *Journal of Structural Geology* 24: 1861–1884.
- Talbot JY, Faure M, Chen Y, Martelet G. 2005a. Pull-apart emplacement of the Margeride granitic complex (French Massif

- Central). Implications for the late evolution of the Variscan orogen. *Journal of Structural Geology* 27: 1610–1629.
- Talbot JY, Chen Y, Faure M. 2005b. Pluton-dykes relationships from AMS and microstructural studies in a Variscan granite from French Massif Central. *J Geophys Res* 110.
- Thompson JFH, Sillitoe RH, Baker T, Lang JR, Mortensen JK. 1999. Intrusion related gold deposits associated with tungsten–tin provinces. *Miner Depos* 34: 323–334.
- Thonat A, Mathonnat M, Pin C, Rocher P, Bertin C, Chèvremont P. 2014. Notice de la carte géologique de France au 1/50 000°, 765. *Massiac* 141 p.
- Vermeesch P. 2018. IsoplotR: a free and open toolbox for geochronology. *Geosci Front* 9: 1479–1493. <https://doi.org/10.1016/J.GSF.2018.04.001>.
- Williams-Jones AE, Bowell RJ, Migdisov AA. 2009. Gold in solution. *Elements* 5: 281–287.
- Wood SA, Samson IM. 2000. The Hydrothermal Geochemistry of Tungsten in Granitoid Environments: I. Relative Solubilities of Ferberite and Scheelite as a Function of T, P, pH, and mNaCl. *Econ Geol* 95: 143–182.
- Zachariáš J, Moravek P, Gadas P, Pertoldova J. 2014. The Mokrsko-West gold deposit, Bohemian Massif, Czech Republic: mineralogy, deposit setting and classification. *Ore Geol Rev* 58: 238–263.
- Petrus DM, Kamber BS. 2014. U-Pb LA-ICPMS dating using accessory mineral standards with variable common Pb. *Chem Geol* 363: 185–199.
- Debon F, Le Fort P. 1988. A cationic classification of common plutonic rocks and their magmatic associations: principles, method, applications. *Bulletin de Minéralogie* 111: 493–510.
- McDowell FW, McIntosh WC, Farley KA. 2005. A precise 40Ar–39Ar reference age for the Durango apatite (U–Th)/He and fission-track dating standard. *Chem Geol* 214: 249–263.
- Paton C, Woodhead JD, Hellstrom JC, Hergt JM, Greig A, Maas R. 2010. Improved laser ablation U-Pb zircon geochronology through robust downhole fractionation correction. *Geochem Geophys Geosyst* 11: Q0AA06.
- Schoene B, Bowring SA. 2006. U-Pb systematics of the McClure Mountain syenite: thermochronological constraints on the age of the 40Ar/39Ar standard MMhb. *Contrib Miner Petrol* 151: 615–630.
- Thomson SN, Gehrels GE, Ruiz J, Buchwaldt R. 2012. Routine low-damage apatite U-Pb dating using laser ablation–multicollector–ICPMS. *Geochem Geophys Geosyst* 13: Q0AA21.

## Pour en savoir plus

**Cite this article as:** Cheval-Garabédian F, Faure M, Marcoux E, Poujol M. 2021. The tungsten-gold veins of Bonnac (French Massif central): new constraints for a Variscan granite-related genesis, *BSGF - Earth Sciences Bulletin* 192: 7.